NEUROSCIENCE

Restoring light sensitivity using tunable near-infrared sensors

Dasha Nelidova[1,2], Rei K. Morikawa[1,2], Cameron S. Cowan[1,2], Zoltan Raics[1,2], David Goldblum[3], Hendrik P. N. Scholl[1,3,4], Tamas Szikra[1,2], Arnold Szabo[5], Daniel Hillier[1,2,6,7,8]*, Botond Roska[1,2,3]*

Enabling near-infrared light sensitivity in a blind human retina may supplement or restore visual function in patients with regional retinal degeneration. We induced near-infrared light sensitivity using gold nanorods bound to temperature-sensitive engineered transient receptor potential (TRP) channels. We expressed mammalian or snake TRP channels in light-insensitive retinal cones in a mouse model of retinal degeneration. Near-infrared stimulation increased activity in cones, ganglion cell layer neurons, and cortical neurons, and enabled mice to perform a learned light-driven behavior. We tuned responses to different wavelengths, by using nanorods of different lengths, and to different radiant powers, by using engineered channels with different temperature thresholds. We targeted TRP channels to human retinas, which allowed the postmortem activation of different cell types by near-infrared light.

Photoreceptor degeneration, including age-related macular degeneration and retinitis pigmentosa, is the leading cause of blindness in industrialized countries. When cone photoreceptors lose light sensitivity, high-resolution vision is affected, and it becomes difficult to carry out the activities of daily living. In most cases, photoreceptor degeneration is incomplete, leading to the presence of light-sensitive and light-insensitive photoreceptor zones next to each other within the same retina. Remaining light-sensitive regions limit the utility of optogenetic (*1*) or light-switch (*2*) therapies, because these technologies require bright, visible light that saturates photoreceptors.

Enabling the detection of near-infrared (NIR) light (>900 nm) at wavelengths outside the spectrum visible to the human eye (390 to 700 nm) could provide a way of supplementing or restoring light sensitivity in the affected retinal region without interfering with the vision that remains. Currently, there is no technology that would allow the induction of NIR sensitivity in a blind retina.

A few species, such as boas, pythons, and pit vipers, can detect infrared light (1 to 30 μm) using temperature-sensitive transient receptor potential (TRP) cation channels expressed in a specialized organ (*3*). Thermal and visual images superimpose in the snake's brain (*4*), presumably enabling the snake to react to the environment with greater precision than what is possible using only a single image. TRP channels could potentially be targeted to retinal cell types to make them sensitive to infrared radiation. However, heat transfer to ectopically expressed TRP channels via direct NIR illumination is inefficient, requiring high intensities that would damage the retina.

To develop a more efficient NIR light detector for retinal cell types, we engineered a dual system consisting of a genetic component and a nanomaterial component (Fig. 1A). The genetic component consisted of temperature-sensitive TRP channels, engineered to incorporate an extracellular epitope recognizable by a specific antibody (*5*). The nanomaterial component consisted of gold nanorods conjugated to an antibody against the epitope (*6*). This system uses surface plasmon resonance for heat transfer (*7*): Gold nanorods capture NIR light at their resonant wavelength and produce heat, which is harnessed to open TRP channels in the proximity of the nanorods. The epitope ensures nanorod binding to engineered rather than native TRP channels, because some TRP channels are expressed in the retina (*8*, *9*).

We developed a system based on rat TRP family V member 1 (TRPV1) channels and gold nanorods with absorption maxima (λ_{abs}) at 915 nm; this value was selected to ensure low water absorption. We inserted a 6x-His epitope tag in the middle of the first TRPV1 extracellular loop (Fig. 1, C and D), after amino acid 459 or 465 (fig. S1). Analysis of TRPV1 structure suggested that insertion at these sites would not disrupt protein function.

To measure whether tagged channels were functional, we performed whole-cell voltage clamp in human embryonic kidney (HEK) cells expressing TRPV1.459-6x-His, TRPV1.465-6x-His, or untagged TRPV1 while activating the channels by TRPV1 agonist capsaicin. The sizes of evoked currents were similar between TRPV1.465-6x-His and TRPV1 (table S1, row A) but smaller in TRPV1.459-6x-His (table S1, row B, and fig. S2). Therefore, we used TRPV1.465-6x-His (abbreviated as rTRPV1) in subsequent experiments.

We targeted rTRPV1 to cone photoreceptors of *Pde6b*^{rd1} mice (known as rd1 mice) through subretinal injection of adeno-associated virus (AAV), using a photoreceptor-specific mouse cone arrestin promoter (mCar) to restrict expression (Fig. 1E). Rd1 mice have severe photoreceptor degeneration, with complete loss of rods and dysfunctional, light-insensitive cone photoreceptors by 4 weeks of age (Fig. 1B) (*10*). Cell membrane expression of rTRPV1 was seen in 55 ± 10% of rd1 cones (table S1, row C, and Fig. 1F). Among rTRPV1-positive cells, 98 ± 1.6% were cones (table S1, row D); these rTRPV1-positive cones expressed the 6x-His tag (table S1, row E, and Fig. 1, E and F).

To measure whether NIR light drives responses in rd1 retinas, we performed two-photon calcium imaging of individual cone cell bodies and axon terminals as well as ganglion cell bodies in wholemount P56-P72 retinas under two conditions: (i) rTRPV1 with nanorods (λ_{abs} = 915 nm) and (ii) rTRPV1 without nanorods. To measure whether NIR light affects normal cones, we performed two-photon calcium imaging of cone axon terminals in wholemount wild-type retinas stimulating cones with NIR (915 nm) and/or visible light. To detect calcium signals in cones, we genetically targeted the calcium indicator GCaMP6s via an AAV that expresses GCaMP6s under a cone-specific promoter (*11*). For ganglion cells, we used the organic calcium sensor Oregon Green 488 BAPTA-1 (OGB-1).

rTRPV1-expressing rd1 cones showed 915-nm light ("NIR light")–evoked increases of calcium signal in the presence of nanorods ("NIR cone response") (Fig. 1, G to I). NIR cone response was of opposite polarity compared with the visible light response of wild-type cones (Fig. 1G). Polarity reversal was due to cation selectivity of rTRPV1. NIR cone response was similar in size to the visible light response of wild-type cones (table S1, rows F and G). NIR light neither activated wild-type cones nor affected their visible light responses (fig. S3). rTRPV1-expressing cones without nanorods did not react to light (Fig. 1, G to I). In the presence of nanorods, NIR light also induced responses in neurons of the ganglion cell layer (GCL) (fig. S4). In all subsequent experiments, we used both the TRP channel and the nanorod component ("NIR sensor"); uninjected rd1 mice were used as the control.

To assess whether NIR light–induced retinal activity propagates to higher visual centers, we generated rd1 mice with targeted GCaMP6s expression in layer 4 of the primary visual cortex (V1). Layer 4 receives feedforward connections from the lateral geniculate nucleus. We performed two-photon calcium imaging

[1]Institute of Molecular and Clinical Ophthalmology Basel, Basel, Switzerland. [2]Friedrich Miescher Institute for Biomedical Research, Basel, Switzerland. [3]Department of Ophthalmology, University of Basel, Basel, Switzerland. [4]Wilmer Eye Institute, Johns Hopkins University, Baltimore, MD, USA. [5]Department of Anatomy, Semmelweis University, Budapest, Hungary. [6]Deutsches Primatzentrum, Leibniz Institute for Primate Research, Göttingen, Germany. [7]Research Centre for Natural Sciences, Budapest, Hungary. [8]Faculty of Information Technology and Bionics, Pázmány Péter Catholic University, Budapest, Hungary.
*Corresponding author. Email: daniel.hillier@iob.ch (D.H.); botond.roska@iob.ch (B.R.)

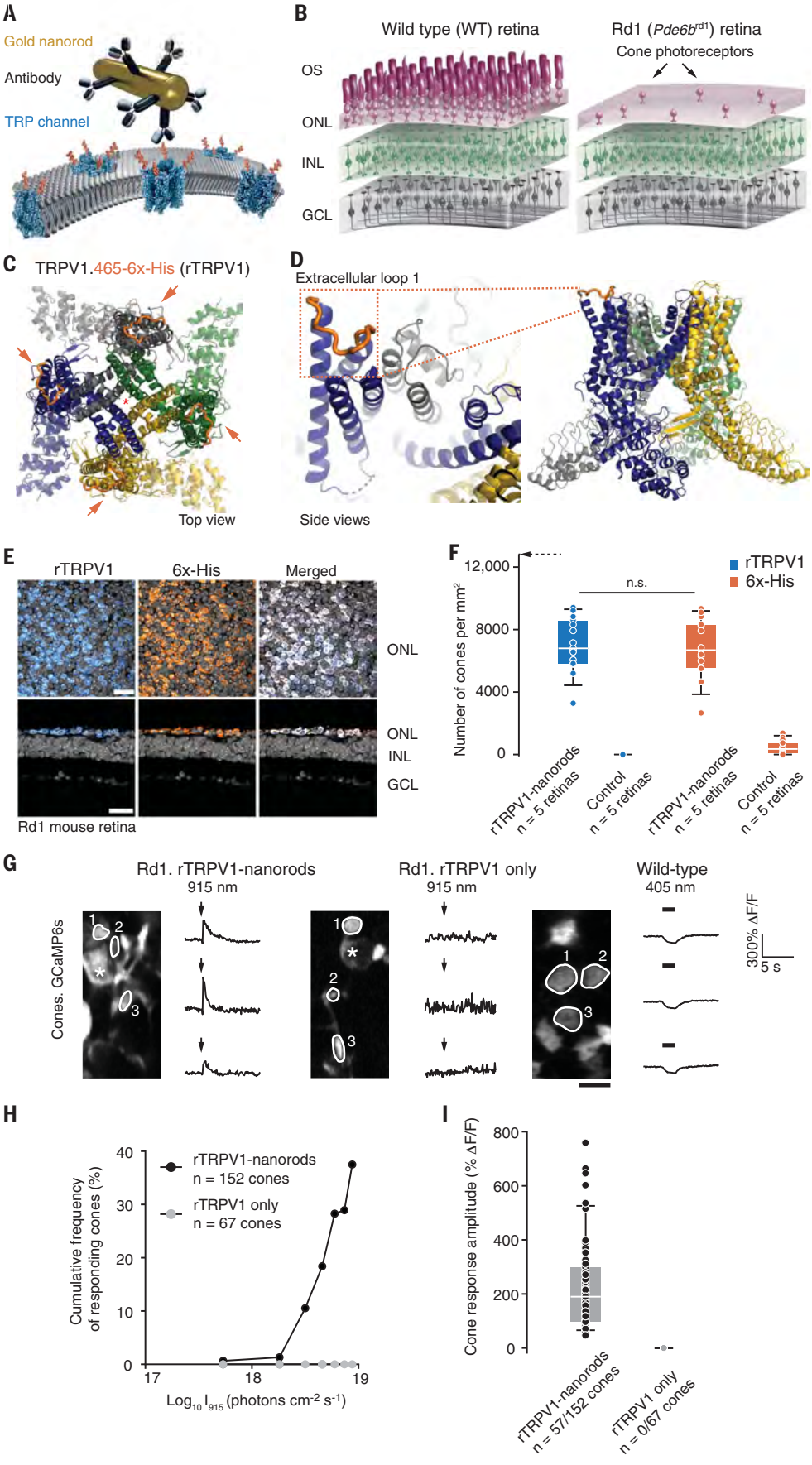

Fig. 1. NIR light responses in mouse cone photoreceptors. (**A**) Components of the NIR light sensor. Engineered TRP channels (blue) express protein epitope tags (orange) in extracellular domains and bind antibody-conjugated gold nanorods. (**B**) Left: Healthy retina. Photons are captured by outer segments (OS) of photoreceptor cells. Right: retinal degeneration, characterized by loss of OS and blindness. In the rd1 mouse model of degeneration, rod cell bodies are lost but cone cell bodies persist. ONL, outer nuclear layer; INL, inner nuclear layer; GCL, ganglion cell layer. (**C** and **D**) Structure of rTRPV1 channel. (C) Top view. Orange arrows indicate a 6x-His epitope tag in each of the four subunits of the TRPV1 tetramer (yellow, blue, gray, and green). The red asterisk marks the channel pore. (D) Right: Side view. Left: 6x-His epitope tag (orange) within the first extracellular loop of the blue subunit is enlarged. (**E**) Top row: Top views of rd1 retinas transduced with both rTRPV1 and nanorods and immunostained for TRPV1 (left, blue), 6x-His (middle, orange), and merging the two (right). Gray, Hoechst nuclear stain. Bottom row: Cross sections of the retinas shown in the top row. Scale bars, 25 μm. (**F**) Number of rTRPV1-positive (blue) and 6x-His–positive (orange) cones per square millimeter in rd1 retinas transduced with both rTRPV1 and nanorods (n = 5 mice) or in control, uninjected rd1 retinas (n = 5 mice). Dashed arrow indicates maximum cone density in rd1 mice at postnatal day 70 (*10*). Each data point is collected from a different region of a retina (three regions per retina). (**G**) Example calcium responses (mean $\Delta F/F$, where F represents baseline fluorescence; two to three repetitions) recorded from cone axon terminals in P56-P71 rd1 mice transduced with rTRPV1 and nanorods (left, λ_{abs} nanorod = 915 nm), in rd1 mice transduced with rTRPV1 only (middle), or in wild-type mice (right). TRP, n = 4 mice; wild-type, n = 3 mice. Stimulus, full-field NIR light (915 nm, $\log_{10}$ light intensity = 18.9; left and middle) or visible light (405 nm, $\log_{10}$ light intensity = 14; right). Black bars (2 s) and arrows (100 ms) indicate stimulus timing. Two-photon images of GCaMP6s-expressing cone axon terminals (white circles) are shown to the left of the response curves. Scale bar, 5 μm. White asterisks indicate cell bodies. (**H**) Cumulative frequency of responding rTRPV1-transduced rd1 cones with (black) and without (gray) nanorods (λ_{abs} = 915 nm). (**I**) Cone response amplitudes ($\Delta F/F$). Light intensities as in (G). Number of cones given as a ratio of responding cones to measured cones.

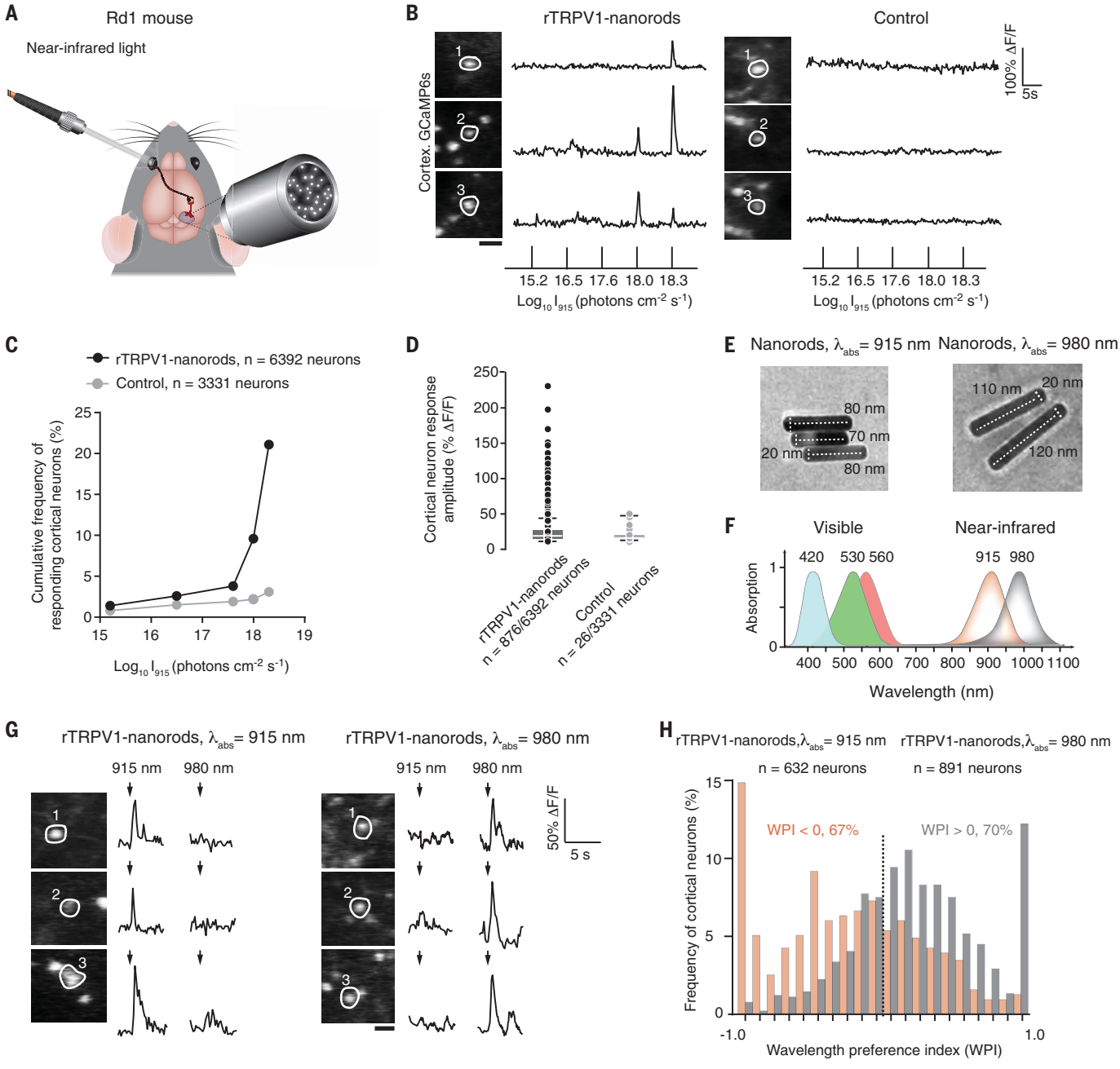

Fig. 2. NIR light responses in mouse primary visual cortex. (**A**) Schematic of the experiments in the primary visual cortex (V1). Cortical neuron calcium responses to 100-ms full-field NIR light stimulation of the contralateral eye were recorded in P51-P83 rd1 mice. (**B**) Example calcium responses (mean $\Delta F/F$, five repetitions) to 915-nm light stimulation recorded in rd1 mice transduced with rTRPV1 and nanorods (left, λ_{abs} = 915 nm, n = 3 mice) and in control, uninjected rd1 mice (right, n = 5 mice). Vertical lines at bottom indicate stimulus timing. Two-photon images of GCaMP6s-expressing neuronal cell bodies in layer 4 of V1 (white circles) are shown to the left of the response curves. Scale bar, 25 μm. (**C**) Cumulative frequency of responding cortical neurons in mice transduced with both rTRPV1 and nanorods (black, λ_{abs} = 915 nm) and in control, uninjected mice (gray). (**D**) Cortical neuron response amplitudes ($\Delta F/F$). Log_{10} light intensity = 18.3. Number of neurons given as ratio of responding neurons to measured neurons. (**E**) Morphology of nanorods tuned to 915 nm (left) and 980 nm (right), measured by transmission electron microscopy. (**F**) Schematic showing nanorod absorption spectra relative to visual pigment of the human retina. (**G**) Example cortical calcium responses (mean $\Delta F/F$, five repetitions) to 915-nm and 980-nm light stimulation (log_{10} light intensity = 18.3). Left: Mice transduced with rTRPV1 and nanorods with λ_{abs} = 915 nm (n = 3 mice). Right: Mice transduced with rTRPV1 and nanorods with λ_{abs} = 980 nm (n = 4 mice). Arrows indicate stimulus timing. Two-photon images of GCaMP6s-expressing neuronal cell bodies in layer 4 of V1 (white circles) are shown to the left of the response curves. Scale bar, 25 μm. (**H**) Frequency of cortical neurons as a function of the WPI in mice transduced with rTRPV1 and nanorods with λ_{abs} = 915 nm (orange) or nanorods with λ_{abs} = 980 nm (gray). For nanorods with λ_{abs} = 915 nm, larger fraction of 915 nm (WPI < 0) over 980 nm (WPI > 0) light preferring neurons. For nanorods with λ_{abs} = 980 nm, larger fraction of 980 nm (WPI > 0) over 915 nm (WPI < 0) light preferring neurons. Light intensities as in (G).

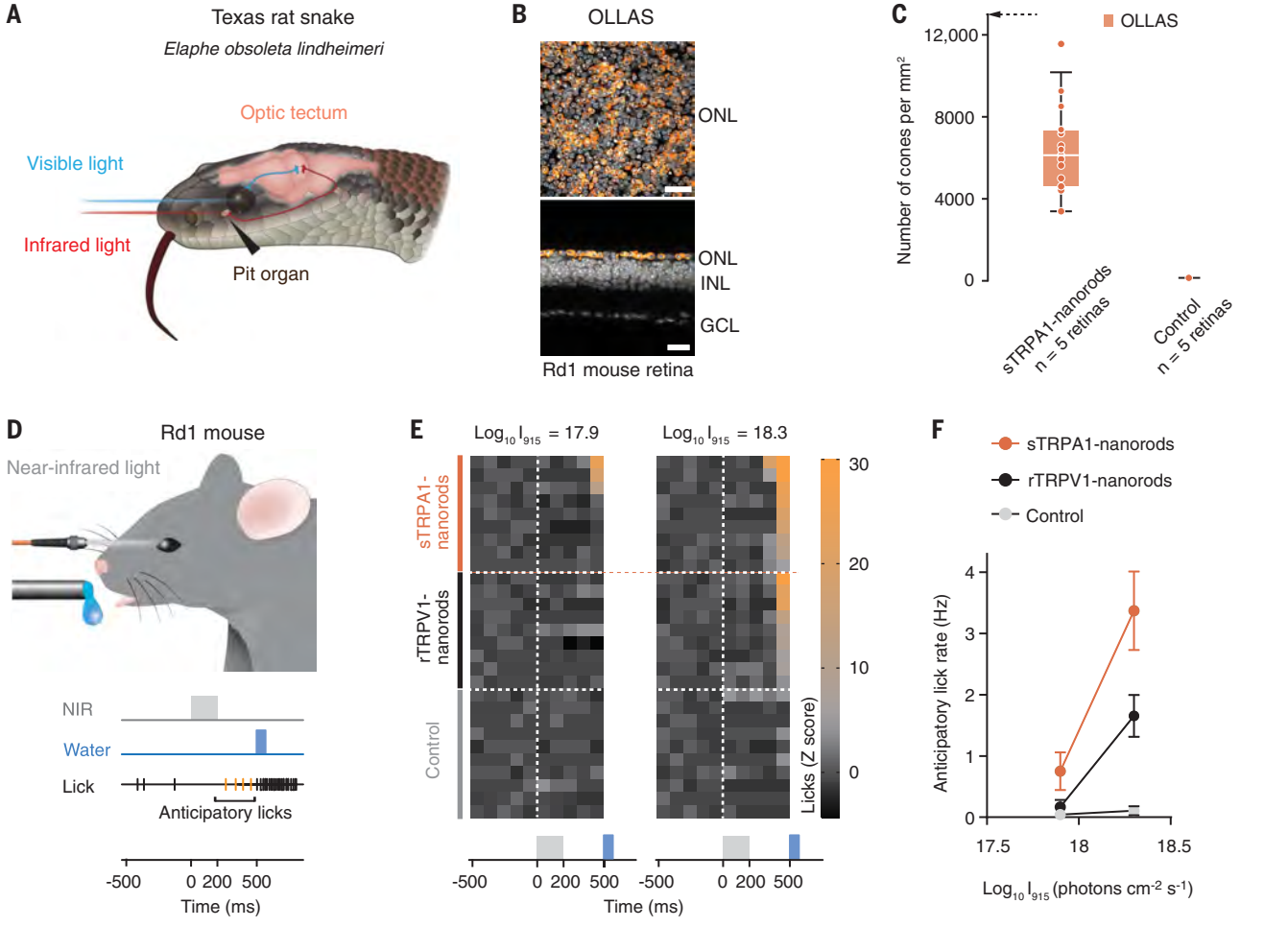

Fig. 3. NIR light–guided mouse behavior. (**A**) Schematic showing location of TRP channel–expressing, infrared-sensitive pit organ. Information is overlaid in the optic tectum. (**B**) Expression of sTRPA1 in cones of rd1 mice. Top: Top view of a retina transduced with both sTRPA1 and nanorods, immunostained for OLLAS (orange) and overlaid with Hoechst nuclear stain (gray). Bottom: Cross section of the retina shown in top image. Scale bars, 25 μm. (**C**) Number of OLLAS-positive (orange) cones per square millimeter in rd1 retinas transduced with both sTRPA1 and nanorods (n = 5 mice) or in control, uninjected rd1 retinas (n = 5 mice). Dashed arrow indicates maximum cone density in rd1 mice at postnatal day 70 (*10*). Each data point is collected from a different region of a retina (three regions per retina). (**D**) Schematic of behavioral task. NIR full-field stimulation of one eye (915 nm, 200 ms) cues water presentation for head-fixed, water-restricted P56-P73 rd1 animals. Mice respond by licking before (anticipation) or after the appearance of water. (**E**) Lick response heatmaps. Rows: Responses of different mice. Columns: Responses in 100-ms time bins. Top: rd1 mice transduced with both sTRPA1 and nanorods (λ_{abs} = 915 nm, n = 9 mice). Middle: rd1 mice transduced with both rTRPV1 and nanorods (λ_{abs} = 915 nm, n = 9 mice). Bottom: Control, uninjected rd1 mice (n = 10 mice). Left: Stimulus $\log_{10}$ light intensity = 17.9. Right: Stimulus $\log_{10}$ light intensity = 18.3. (**F**) Mean anticipatory lick rates quantified from (E) as a function of light intensity. Error bars, SEM.

in vivo in P51-P83 animals, recording layer 4 activity at single-cell resolution during NIR light stimulation of the eye (Fig. 2A). In NIR sensor–injected animals, cortical neurons showed NIR light–evoked increases in calcium signal (Fig. 2B), which were light-intensity dependent (Fig. 2C and fig. S5). Neuronal activation was greater in NIR sensor–injected animals than in controls (table S1, row H, and Fig. 2C).

Nanorod absorption spectra can be wavelength-tuned by varying nanorod aspect ratios (length-to-width ratios) (Fig. 2E and fig. S6). To test whether the action spectra of neuronal activity can also be tuned, we selected a second type of gold nanorod with peak absorption at 980 nm (aspect ratio: 5.5) and compared with nanorods with peak absorption at 915 nm (aspect ratio: 4.0). Both types were paired to rTRPV1. For each nanorod type, we performed layer 4 cortical calcium imaging in P51-P71 rd1 mice twice: once with 980-nm stimulation of the eye, and once with 915-nm stimulation. To classify cortical neurons as 980 nm or 915 nm responsive, we computed a wavelength preference index (WPI) for each NIR light–responsive neuron. We found a preference for 980-nm light over 915-nm light using nanorods tuned to 980 nm (table S1, row I; Fig. 2H; and fig. S7). Similarly, in animals with nanorods tuned to 915 nm, more cortical neurons preferred 915-nm light over 980-nm light (table S1, row J; Fig. 2H; and fig. S7).

Next, we asked whether molecular components can be tuned to increase sensitivity. A variety of TRPA1 channels also serve as heat sensors. TRPA1 from the Texas rat snake (*Elaphe obsoleta lindheimeri*) is activated at a lower temperature than rTRPV1 (*3*). To determine the suitability of snake TRPA1 as a NIR sensor component, we first engineered TRPA1 to express the peptide epitope tag OLLAS (*12*) within the first or second extracellular loop. Anti-OLLAS antibodies show improved immunodetection compared with anti-6x-His and other antibodies for conventional epitope tags (*12*). To identify loop domains, we first determined the location of extracellular loop domains of human TRPA1 from its cryo–electron microscopy structure (*13*). Subsequently, we identified potential loop domains of snake TRPA1 after pairwise sequence

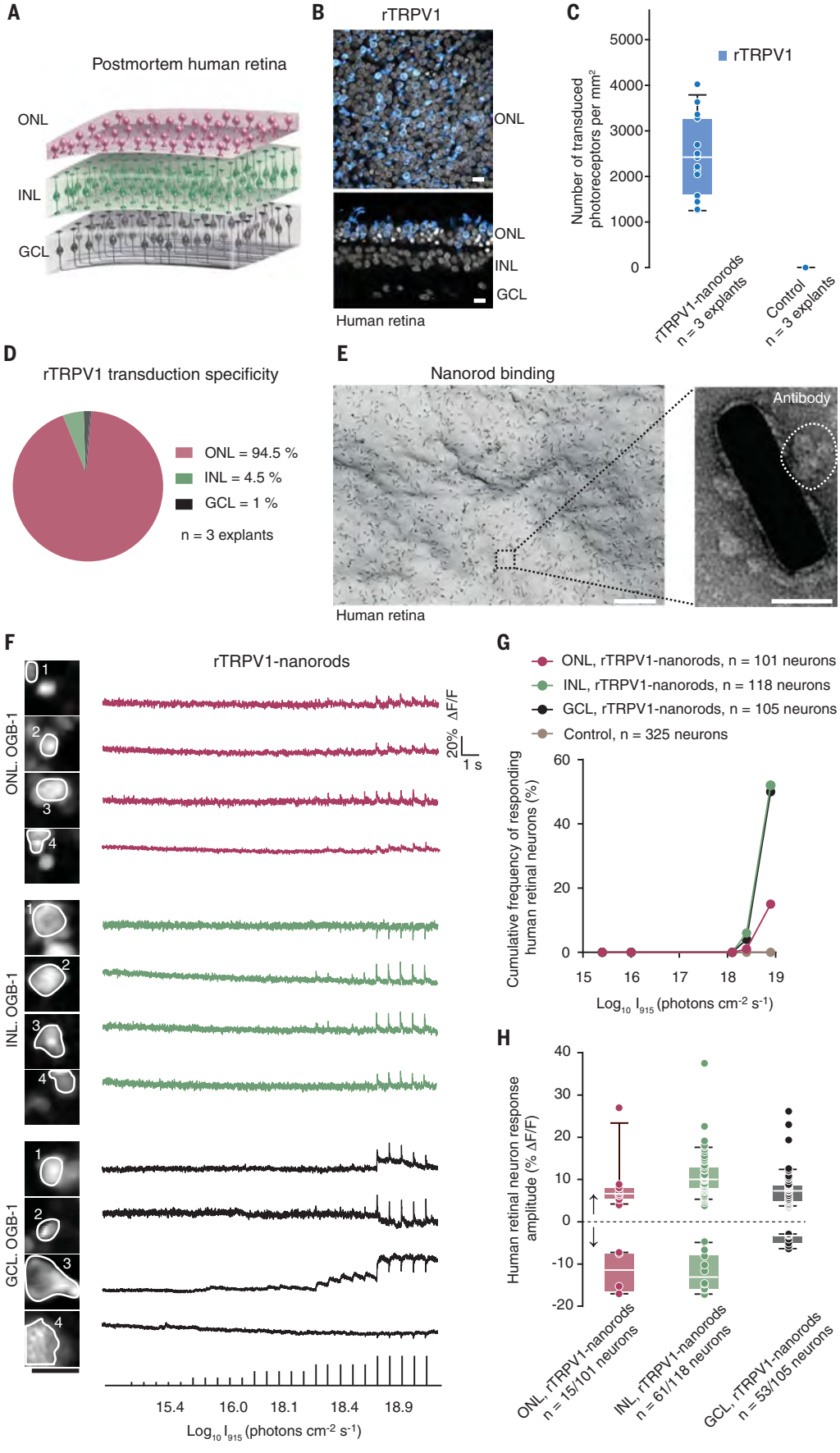

Fig. 4. NIR light responses in the ex vivo human retina. (**A**) Schematic of a human retinal explant 8 weeks postmortem. Long-term culture leads to loss of outer segments and light responses. (**B**) Top: Top view of a human retina transduced with both rTRPV1 and nanorods, immunostained for TRPV1 (blue) and overlaid with Hoechst nuclear stain (gray). Bottom: Cross section of the retina shown in top image. Scale bars, 10 μm. (**C**) Number of rTRPV1-positive (blue) photoreceptors per square millimeter in human retinas transduced with both rTRPV1 and nanorods or in control, untransduced human retinas. Each data point is collected from a different region of a retina (five regions per retina). (**D**) Distribution of rTRPV1-positive cells across retinal layers. (**E**) Scanning electron microscopy image of gold nanorods bound to a rTRPV1-transduced human retina. Scale bar, 1 μm. Inset: Transmission electron microscopy image showing an anti-6x-His antibody touching a gold nanorod with its Fc domain. Scale bar, 20 nm. (**F**) Example calcium responses recorded from human retinal neurons in ONL, INL, and GCL in response to full-field NIR light. Vertical lines at bottom indicate stimulus (915 nm, 100 ms) timing. Two-photon images of OGB-1 filled cell bodies (white circles), left of the response curves. Scale bar, 10 μm. (**G**) Cumulative frequency of responding neurons in different layers of human retinas transduced with both rTRPV1 and nanorods (λ_{abs} = 915 nm) or in control, untransduced human retinas. (**H**) Response amplitudes ($\Delta F/F$) by retinal layer. Increase (↑) and decrease (↓) of calcium signal are shown separately. Number of neurons given as ratio of responding neurons to measured neurons. Log_{10} light intensity = 18.9.

alignment (*14*) between human and snake sequences. OLLAS was placed after amino acid 755 or 758, corresponding to the first loop, or after amino acid 824, corresponding to the second loop (fig. S8).

We performed whole-cell voltage clamp in HEK cells expressing TRPA1.755-OLLAS, TRPA1.758-OLLAS, TRPA1.824-OLLAS, or untagged TRPA1 while activating the channels by TRPA1 agonist allyl isothiocyanate. The sizes of evoked currents were similar between TRPA1.755-OLLAS and TRPA1 (table S1, row K) and between TRPA1.824-OLLAS and TRPA1 (table S1, row L, and fig. S9). Currents were undetectable for TRPA1.758-OLLAS (fig. S9B). We used TRPA1.755-OLLAS (abbreviated as sTRPA1) in subsequent experiments.

We targeted sTRPA1 to cone photoreceptors of rd1 mice using the same AAV-based approach that was used for rTRPV1 (Fig. 3). To activate the channel, nanorods (λ_{abs} = 915 nm) were conjugated to anti-OLLAS antibodies. Cell membrane expression of sTRPA1 was seen in 50 ± 13% of rd1 cone photoreceptors (table S1, row M, and Fig. 3C). Cones made up 99 ± 0.8% of OLLAS-positive cells (table S1, row N).

To compare rTRPV1 and sTRPA1 sensitivities, we performed behavioral tests in NIR sensor–injected P56-P73 rd1 mice. NIR light of two different intensities cued delayed water appearance for water-restricted, head-fixed animals (Fig. 3D). We evaluated anticipatory lick rates, defined as lick signal after a NIR light flash but before the appearance of water. To measure whether NIR light affects the behavior of wild-type animals, we trained wild-type mice with NIR (915 or 980 nm) and/or visible light (fig. S10A). NIR sensor–injected mice learned to associate NIR light with water within 4 days. At the lower NIR intensity, anticipatory lick rates were similar between control mice and mice with rTRPV1 (table S1, row O) but higher for mice injected with sTRPA1 (table S1, row P, and Fig. 3, E and F). At the higher NIR intensity, rTRPV1 led to higher lick rates compared with control mice (table S1, row Q), but lower than with sTRPA1 (table S1, row R, and Fig. 3, E and F). Behavioral performance of rTRPV1 and sTRPA1 mice was similar to that of wild-type mice trained for 4 days using visible light (table S1, rows S and T, and fig. S10). NIR light neither elicited behavioral responses in wild-type mice nor affected wild-type behavioral responses to visible light (fig. S10C).

To test safety aspects of inducing NIR light sensitivity, we first evaluated the effect of prolonged NIR light exposure on wild-type retinas by immunostaining. NIR light neither activated microglia nor reduced retinal layer thickness, opsin density, or cone density (fig. S11). Second, we tested nanorod biocompatibility with the rd1 retina 80 and 100 days after subretinal injection by immunostaining. Nanorods neither activated microglia, increased apoptosis, nor reduced retinal layer thickness (fig. S12).

Finally, we sought to induce NIR light sensitivity in blind human retinas (Fig. 4). We targeted rTRPV1 to adult human ex vivo retinal explants, in culture for 8 weeks postmortem (Fig. 4B and fig. S13). Retinas lose normal light–evoked activity within 24 hours of isolation (*15*). Using AAV delivery and a CAG promoter, we transduced 2477 ± 889 photoreceptors per square millimeter of human retina (mean ± SD, n = 3 explants) with rTRPV1 (Fig. 4C). Of the rTRPV1-positive cells, 94.5 ± 4.2% were photoreceptors (table S1, row U, and Fig. 4D). To measure whether NIR light drives responses in the human retina, we deposited nanorods (λ_{abs} = 915 nm) over the photoreceptor side. To record calcium signals, we used the fluorescent calcium dye OGB-1 (*16*, *17*). We then performed two-photon calcium imaging of individual neurons in the outer nuclear layer (ONL), inner nuclear layer (INL), and GCL (Fig. 4A). We observed NIR light–induced activation of different human retinal cell classes (Fig. 4, F to H). Most photoreceptors (73%) showed NIR light–evoked increases of calcium signal (Fig. 4H). Some photoreceptors (27%) showed decreases of calcium signal, likely reflecting horizontal cell feedback to NIR light–insensitive photoreceptors (Fig. 4H). In neurons of the INL and GCL, we observed both increases and decreases in calcium signal, indicating activation of excitatory and inhibitory retinal pathways (Fig. 4H). More cells responded in the GCL than in the ONL, reflecting convergent retinal circuit organization (Fig. 4G). Sizes of light-evoked calcium responses were comparable to those in published reports (*16*, *17*).

Here, we described an approach to enable NIR light sensitivity in blind retinas, designed to be compatible with remaining vision (see supplementary text). We used gold nanorods coupled to temperature-sensitive engineered TRP channels to induce NIR light sensitivity in remaining photoreceptor cell bodies of blind mice and in ex vivo human retinas. In mice, NIR light–sensitized photoreceptors activated cortical visual circuits and enabled behavioral responses. By means of distinct nanorods, epitope tags, and TRP channel types, we tuned NIR responses to different wavelengths and to different radiant powers. In the human retina, we reactivated light responses in photoreceptors and their retinal circuits 8 weeks postmortem. Our recordings of NIR light–evoked activity in the postmortem human retina provide not only proof-of-principle for translation but also a model with which the function of human retinal cell types and circuits can be studied.

REFERENCES AND NOTES

1. J. A. Sahel, B. Roska, *Annu. Rev. Neurosci.* **36**, 467–488 (2013).
2. I. Tochitsky, M. A. Kienzler, E. Isacoff, R. H. Kramer, *Chem. Rev.* **118**, 10748–10773 (2018).
3. E. O. Gracheva *et al.*, *Nature* **464**, 1006–1011 (2010).
4. E. A. Newman, P. H. Hartline, *Science* **213**, 789–791 (1981).
5. S. A. Stanley *et al.*, *Science* **336**, 604–608 (2012).
6. P. P. Joshi, S. J. Yoon, W. G. Hardin, S. Emelianov, K. V. Sokolov, *Bioconjug. Chem.* **24**, 878–888 (2013).
7. Z. Qin, J. C. Bischof, *Chem. Soc. Rev.* **41**, 1191–1217 (2012).
8. M. Lakk *et al.*, *Front. Cell. Neurosci.* **12**, 353 (2018).
9. D. A. Ryskamp, S. Redmon, A. O. Jo, D. Križaj, *Cells* **3**, 914–938 (2014).
10. V. Busskamp *et al.*, *Science* **329**, 413–417 (2010).
11. J. Jüttner *et al.*, *Nat. Neurosci.* **22**, 1345–1356 (2019).
12. S. H. Park *et al.*, *J. Immunol. Methods* **331**, 27–38 (2008).
13. C. E. Paulsen, J. P. Armache, Y. Gao, Y. Cheng, D. Julius, *Nature* **520**, 511–517 (2015).
14. L. Zimmermann *et al.*, *J. Mol. Biol.* **430**, 2237–2243 (2018).
15. C. S. Cowan *et al.*, bioRxiv 703348 [Preprint]. 16 July 2019. https://doi.org/10.1101/703348.
16. K. L. Briggman, T. Euler, *J. Neurophysiol.* **105**, 2601–2609 (2011).
17. T. Baden *et al.*, *Nature* **529**, 345–350 (2016).

ACKNOWLEDGMENTS

We thank organ and tissue donors and their families for their generous contributions to science; T. Vögele, J. Sprachta, and P. Blaschke for organizing organ donations; H. Gut and R. Bunker for advice on TRP channel design; J. Jüttner, C. Patino-Alvarez, Ö. Keles, and N. Ledergerber for technical assistance; J. Krol for advice on molecular assays; E. Macé and F. Esposti for assistance with recordings; P. Argast and P. Buchmann for electrical and mechanical engineering in support of the experiments; K. Franke, T. Euler, and Z. Zhao for advice on loading of calcium indicators by electroporation; F. Müller for statistical advice; W. Baehr for sharing of antibodies; D. Dalkara, C. Cepko, and E. Bamberg for plasmids; FMI and NIBR core facilities for their support, especially the microscopy facility, in particular C. Genoud and A. Graff-Meyer for electron microscopy; V. Juvin from SciArtWork for illustrations; and M. Munz and T. Rodrigues for commenting on the manuscript. **Funding:** This work was supported by a Swiss National Science Foundation Synergia grant, a European Research Council advanced grant, a Louis-Jeantet Foundation award, a Swiss National Science Foundation grant, the NCCR "Molecular Systems Engineering" network, a private donation from Lynn and Diana Lady Dougan to B.R., NKFIH 129120 and 2017-1.2.1-NKP-2017-00002 grants to D.H., and a Swiss Academy of Medical Sciences Fellowship to D.N. **Author contributions:** D.N. designed and performed experiments and wrote the paper. C.S.C. performed human retina recordings. R.K.M. performed mouse photoreceptor recordings. Z.R. wrote software. D.G., H.P.N.S., and A.S. contributed to human retina experiments. T.S. performed HEK cell recordings. D.H. performed cortical recordings and analyzed data. B.R. designed experiments and wrote the paper. **Competing interests:** D.N. and B.R. have a patent application on NIR sensors (EP20158285.5). **Data and materials availability:** TRP plasmid materials are available from B.R. under an agreement with the Institute of Molecular and Clinical Ophthalmology Basel. All data are available in the manuscript or the supplementary materials.

SUPPLEMENTARY MATERIALS

science.sciencemag.org/content/368/6495/1108/suppl/DC1
Materials and Methods
Supplementary Text
Figs. S1 to S13
Tables S1 to S4
References (*18*–*40*)

View/request a protocol for this paper from *Bio-protocol*.

21 September 2019; accepted 9 April 2020
10.1126/science.aaz5887

science.sciencemag.org/content/368/6495/1108/suppl/DC1

Supplementary Materials for

Restoring light sensitivity using tunable near-infrared sensors

Dasha Nelidova, Rei K. Morikawa, Cameron S. Cowan, Zoltan Raics, David Goldblum, Hendrik P. N. Scholl, Tamas Szikra, Arnold Szabo, Daniel Hillier*, Botond Roska*

*Corresponding author. Email: daniel.hillier@iob.ch (D.H.); botond.roska@iob.ch (B.R.)

Published 5 June 2020, *Science* **368**, 1108 (2020)
DOI: 10.1126/science.aaz5887

This PDF file includes:

Materials and Methods

Animals

Wild-type (strain: C57BL/6J, stock number: 632) and rd1 mice (strain: C3H/HeNCrL, stock number: 025) were obtained from Charles River. Scnn1a-Cre mice (strain: B6;C3-Tg(Scnn1a-cre)3Aibs/J, stock number: 009613) and Ai94(TITL-GCaMP6s)-D mice (strain: B6.Cg-Igs7.tm94.1(tetO-GCaMP6s)Hze.IJ, stock: 024104) were purchased from Jackson Laboratory. Ai94(TITL-GCaMP6s)-D mice were initially crossed to Scnn1a-Cre mice to obtain mice hemizygous for each gene. Hemizygous offspring were subsequently crossed to rd1 mice. Mice used for cortical calcium imaging experiments were hemizygous for Cre and GCaMP6s and homozygous for the rd1 mutation. Access to water was restricted for behavioral training but was otherwise freely available. Animal experiments were performed according to standard ethical guidelines and were approved by the Veterinary Department of Canton Basel Stadt.

Human retinal tissue

Human retinal tissue was obtained after corneal tissue procurement from adult multi-organ donors with no reported history of eye disease. All tissue samples were obtained in accordance with the tenets of the Declaration of Helsinki. Personal identifiers were removed and samples were coded before processing. All procedures and experimental protocols were approved by the local ethics committee. The study includes $n = 2$ eyes from $n = 2$ donors. After cornea isolation, the iris, lens, and vitreous were removed and the retina was submerged in flowing Ames' medium (Sigma, A1420) saturated with 95% O_2 and 5% CO_2. Time elapsed from central retinal artery clamp to artificial *ex vivo* perfusion did not exceed 5 min. Samples used for tissue culture were of mid-peripheral origin, midway between the fovea and the anterior retinal border. For organotypic retinal culture, 4×4 mm retinal pieces were isolated and placed photoreceptor-side-up on polycarbonate membranes inserts (Corning, 3412). The cultures were maintained at 37°C and 5% CO_2 in DMEM/F12 medium (Thermo Fisher Scientific), supplemented with 0.1% bovine serum albumin (BSA), 10 µM *O*-acetyl-L-carnitine hydrochloride, 1 mM fumaric acid, 0.5 mM galactose, 1 mM glucose, 0.5 mM glycine, 10 mM HEPES, 0.05 mM mannose, 13 mM sodium bicarbonate, 3 mM taurine, 0.1 mM putrescine dihydrochloride, 0.35 µM retinol, 0.3 µM retinyl acetate, 0.2 µM (+)-α-tocopherol, 0.5 mM ascorbic acid, 0.05 µM sodium selenite, 0.02 µM hydrocortisone, 0.02 µM progesterone, 1 µM insulin, 0.003 µM 3,3′,5-triiodo-L-thyronine, 2 000 U penicillin and 2 mg streptomycin (Sigma). For AAV infection 40 µL of virus was applied per retinal explant 4–5 days after plating. The culture medium was renewed every 48 hours. Light responses were recorded from samples 8 weeks post-mortem.

Nanorods

Gold nanorods tuned to 915 nm or 980 nm were purchased from Nanopartz Inc (Loveland, USA) and were functionalized by conjugation to anti-Histidine (Millipore, mouse monoclonal anti-polyHis, 05949) or anti-Ollas (Novus Biologicals, rat monoclonal anti-Ollas epitope tag L2, NBP1-06713) antibodies. 10^{10} nanorods were administrated per eye. Additional nanorod related information can be found in Table S2.

TRP channel design

Rat TRPV1 (NM 031982.1) and snake *Elaphe (Pantherophis) obsoleta lindheimeri* TRPA1 (GU 562966) open reading frame sequences were chemically synthesized by Genewiz Inc (South Plainfield, USA). The snake sequence was codon optimized for *Mus musculus* (Java Codon Adaptation Tool, www.jcat.de). Rat TRPV1 protein was tagged by 6x-His introduced in the first extracellular loop, after amino acid 459 or 465. Extracellular loop location was determined based on the cryo-EM structure of rat TRPV1 (PDB 3J5P) (*18*). Snake TRPA1 protein was tagged by Ollas (SGFANELGPRLMGK) (*12*) flanked by GSG linkers, introduced after amino acid 755 or 758 (first loop) or 824 (second loop). To identify loop domains, first, the location of extracellular loop domains of human TRPA1 (PDB 3J9P) were determined from its cryo-EM structure (*13*). Subsequently, predicted loop domains of snake TRPA1 were identified after pairwise sequence alignment, generated using HHPRED (*14*), between C-terminal domains of human (Uniprot O75762) and snake TRPA1 (Uniprot D4P382).

Plasmids

For *in vitro* HEK293T cell experiments, sequences encoding TRP variants were fused to T2A self-cleaving peptide (LEGRGSLLTCGDVEENPGPAPGST) and either mCherry or GFP fluorescent protein. Variants were inserted into linearized pAAV-EF1a-CatCh-GFP plasmid via restriction sites and homologous recombination, replacing the CatCh-GFP sequence. pAAV-EF1a-CatCh-GFP plasmid was constructed by adaptor PCR and the Clontech In-Fusion kit using pcDNA3.1(-)-CatCh-GFP (a kind gift of E. Bamberg, MPI, Frankfurt) and pAAV-EF1a-GFP (B. Roska lab plasmid collection). To generate pAAV-mCAR-TRPV1.465-6x-His (rTRPV1), plasmid pAAV-mCar-MAC-mCherry (B. Roska lab plasmid collection) was linearized with NotI/HindIII. Subsequently, PCR amplified TRPV1.465-6x-His (from pAAV-EF1a-TRPV1.465-6x-His-T2A-mCherry) was inserted, replacing the MAC-mCherry sequence. To generate pAAV-mCAR-TRPA1.755-Ollas (sTRPA1), plasmid pAAV-mCar-MAC-mCherry was linearized with NotI/MluI. Subsequently, PCR amplified TRPA1.755-Ollas (from pAAV-EF1a-TRPA1.755-Ollas-T2A-mCherry) was inserted, replacing the MAC-mCherry sequence. To generate pAAV-CAG-TRPV1.465-6x-His, plasmid pAAV-CAG-ChrimsonR-tdtomato (a kind gift of D. Dalkara, Vision Institute, Paris) was linearized with ClaI/HindIII. Subsequently, PCR amplified TRPV1.465-6x-His (from pAAV-EF1a-TRPV1.465-6x-His-T2A-mCherry) was inserted, replacing the ChrimsonR-tdtomato sequence. The names of TRP plasmids generated are listed in Table S3. To induce GCaMP6s expression in cortical experiments, AAV-pCAG-FLEX2-tTA2 plasmid was obtained from Addgene (65458).

AAV production

AAV production was carried out as described previously (*11*). Briefly, HEK293T cells were co-transfected with an AAV transgene plasmid, an AAV helper plasmid encoding the AAV Rep2 and Cap proteins for the selected serotype, and the pHGT1-Adeno1 helper plasmid harboring adenoviral genes (kindly provided by C. Cepko, Harvard Medical School, Boston) using branched polyethyleneimine (PEI, Polysciences). The AAVs were isolated using a discontinuous iodixanol gradient (OptiPrep, Sigma, D1556) and ultracentrifugation. AAV particles were purified and concentrated in Millipore Amicon 100K columns. Genome copy number titration was performed

using real-time PCR (Applied Biosystems, TaqMan reagents). AAVs were used when titer was equal to or greater than 10^{13} genome copies per mL. We used serotype BP2 to deliver TRP channels to photoreceptors (*19*). To induce GCaMP6s expression in cortical experiments, serotype PHP.eB (*20*) was used to deliver AAV-pCAG-FLEX2-tTA2.

Injections

Ocular injections to deliver AAVs with TRP transgenes were performed on ~4 week old mice anesthetized with 2.5% isoflurane. When required, nanorods were co-injected. A small incision was made with a sharp 30 gauge needle at the nasal corneoscleral junction and AAV, with or without nanorods, was injected through this incision into the subretinal space using a blunt 5 µL Hamilton syringe held in a micromanipulator. For cone photoreceptor activity monitoring, cone specific AAV-GCaMP6s was co-injected subretinally with rTRPV1 AAV. A maximum volume of 2.5 µL was administered per eye. For primary visual cortex activity monitoring, AAV-pCAG-FLEX2-tTA2 was delivered by intravenous retro-orbital injection as previously described (*21*) 2 weeks after initial ocular injection of rTRPV1 and nanorods. There was a minimum incubation time of 3 weeks after intraocular injection before performing experiments on AAV injected animals.

Surgery for *in vivo* two-photon imaging and behavior

Craniotomy surgery for *in vivo* two-photon imaging was performed as described previously (*21*). Briefly, mice were anesthetized with a mixture of fentanyl (Mepha) (0.05 mg/kg), medetomidine (Virbac) (0.5 mg/kg) and midazolam (Roche) (5.0 mg/kg) and were head-fixed in a stereotaxic frame (Narishige, SR-5M-HT). A circular craniotomy of ~3.5 mm diameter was made above the primary visual cortex. After removal of the skull flap, the cortical surface was kept moist with a cortex buffer containing 125 mM NaCl, 5 mM KCl, 10 mM glucose, 10 mM HEPES, 2 mM $MgSO_4$ and 2 mM $CaCl_2$. The cortex was then covered with a 3 mm diameter glass coverslip and sealed with dental acrylic cement (Paladur, Kulzer). A metal bar for head fixation during imaging was glued to the skull (Vetbond, 3M) followed by further dental cement treatment. For behavioral experiments, a custom-made titanium headbar was attached to the skull with tissue adhesive and dental cement.

HEK293T cell current recordings

For HEK293T cell experiments, cells were maintained at 37°C on poly-D-lysine/laminin coated coverslips (GG-12-Laminin, Neuvitro) in DMEM supplemented with 10% fetal bovine serum. Cells were transfected with plasmids containing TRP variants using branched PEI. Cells were perfused in oxygenated Ringer's medium containing 110 mM NaCl, 2.5 mM KCl, 1 mM $CaCl_2$, 1.6 mM $MgCl_2$, 10 mM D-glucose and 22 mM $NaHCO_3$ at ~36°C for the duration of the experiment. Recordings were made in whole-cell voltage clamp mode with borosilicate pipettes (Sutter Instrument Company) pulled to between 4–6 MΩ resistance, voltage clamping the cells to −60 mV. The intracellular solution contained 115 mM potassium gluconate, 9.7 mM KCl, 1 mM $MgCl_2$, 0.5 mM $CaCl_2$, 1.5 mM EGTA, 10 mM HEPES, 4 mM ATP-Na_2, 0.5 GTP-Na_2 at pH 7.2. For comparison of currents between tagged and untagged channels, TRPV1 agonist capsaicin (Sigma, 360376) and TRPA1 agonist allyl isothiocyanate (AITC, Sigma, W203408) were bath

applied at 2.5 μM and 700 μM, respectively, using a valve system (VC-6, Warner Instruments). Electrophysiological recordings were made using an Axon Multiclamp 700B amplifier (Molecular Devices). Signals were digitized at 10 kHz (National Instruments). Data was analyzed offline using MATLAB (MathWorks).

Near-infrared stimulation

Near-infrared (NIR) pulses were produced by two custom-made, single wavelength NIR diode lasers emitting at 915 nm or 980 nm, modelled after (*22*). The laser diode was driven by a pulsed quasi-CW current power supply (Lumina Power, Bradford, USA). The controller had a rise time of 25 μs. Laser emission from the diode was collimated using an aspherical lens (f ¼ 11.5 mm, 0.25 NA). For *ex vivo* retinal experiments, laser output was launched into a fiber optic patch cable (Thorlabs, M79L01) interconnected with a fiber optic cannula (Thorlabs, CFM14L20) (both 400 μm, 0.39 NA). The cannula was positioned 300 μm above and 300 μm lateral to the imaging plane, at angle of 30–35°. Full-field, 100 ms pulses were delivered every 2–10 s. For *in vivo* cortical and behavioral experiments lasers were connected to a fiber optic patch cable positioned 6 mm from the cornea (550 μm, 0.22 NA) (Thorlabs, M37L02). A visible laser line (532 nm), coupled to both NIR lasers, aided alignment over the center of the pupil. Full-field, 100 ms or 200 ms pulses were delivered every 1–30 s. Total laser power output, as a function of driving voltage, was measured by placing cannula (CFM14L20) and patch cable (M37L02) output at the entrance of an integrating sphere photodiode power sensor (Thorlabs, S142C) with a PM100D read-out unit. Oscilloscope read-out of laser response time was obtained by applying a step control voltage to the lasers. Light intensities are indicated in the text and in Table S4.

Two-photon calcium imaging of mouse cone photoreceptors

Wild-type and rd1 retinas were isolated in oxygenated Ringer's medium. For cone photoreceptor calcium-based activity monitoring mouse retinas were mounted ganglion cell-layer-up on filter paper (MF-membrane, Millipore, HAWP01300) with a 2×2 mm aperture to allow for light stimulation of the photoreceptors. To expose photoreceptors, the pigment epithelium layer was peeled away. In rd1 experiments, nanorods were reapplied to the photoreceptor side after peeling (10^{10} nanorods). During imaging, the retina was continuously perfused with oxygenated Ringer's medium at ~36°C. The calcium sensor GCaMP6s was targeted to cone photoreceptors virally, using cell-type specific promoter ProA1 or ProA7 (*11*) to restrict expression to cones. GCaMP6s-expressing cone cell bodies and axon terminals were imaged in a wholemount preparation of the retina. NIR light recordings in wild-type cones were made in light adapted retinas. The two-photon microscope system used was equipped with a two-photon laser scanning at 920 nm (Spectra Physics, Santa Clara, USA) and a 60× objective (Fluor, 1.0 NA, Nikon). Images were acquired using software developed by SELS Software (Hungary), taking images of 150×150 pixels at 10 Hz. Fluorescence was analyzed semi-online using software written in Python (*23*). Cone axon terminals and cell bodies were segmented manually. Fluorescence values were then normalized as ΔF/F, where F represents baseline fluorescence (mean fluorescence of a 1–2 s time window before the onset of the stimulus). Full-field, 915 nm, 100 ms stimulus was presented 2–3 times at each intensity. Full-field, 405 nm, 2 s stimulation was used for wild-type cones. Responses to different trials were averaged before calculating peak responses. Responses were analyzed offline using MATLAB. NIR induced rd1 responses were the means of 3 ΔF/F values within 2 s of stimulation

onset, including the maximum value and its immediately adjacent 2 data points. Visible light responses were calculated as the mean of ΔF/F values during the second half of the stimulation period. Cells were considered responsive when Z scores exceeded 1.5 for each of the stimulus repetitions.

Two-photon calcium imaging of mouse retinal ganglion cells

Rd1 retinas were isolated in oxygenated Ringer's medium. Oregon Green 488 Bapta-1 (OGB-1) calcium dye (Invitrogen, O-6806) was bulk electroporated into retinal ganglion cells as described before (*16, 17*). Briefly, the retina was flat mounted on anodisc filter membranes (#13, 0.2 μm pore size, GE Healthcare, Maidstone, UK) ganglion cell-layer-up. Nanorods were added to the photoreceptor side (10^{10} nanorods). Retinas were electroporated between 3 mm horizontal plate electrodes (Sonidel, CUY700P3E) with 10 μL of 5 mM OGB-1 in Ames' medium using 10–12 pulses (9 V, 100 ms, 1 Hz) from TGP110 Pulse Generator (Aim & TTi, Cambridge, England). The tissue was left to recover for 60 min before recording activity. Calcium-based activity was recorded using the same two-photon microscope system as for cone photoreceptor recordings. Full-field, 915 nm, 100 ms stimulus was presented 5 times at each intensity. Fluorescence was analyzed offline using software written in Python. Raw traces were corrected for slow drifts in baseline fluorescence. NIR responses were evaluated using a 3-sample average of the peri-stimulus activity. Peak responses within a 1 s post-stimulus interval were extracted for every trial and averaged. Cells were considered responsive if at least one third of the pairwise Pearson correlation coefficients across repeated trials exceeded 0.25 with $P < 0.05$.

Two-photon calcium imaging in mouse primary visual cortex

For primary visual cortex calcium-based activity monitoring, Cre- and Tet- dependent Ai94-GCaMP6s mice were crossed to Scnn1a-Cre mice and to rd1 mice (see "Animals"). Tetracycline-controlled transactivator (tTA2), delivered by intravenous retro-orbital injection (see "Injections"), induced layer 4 specific GCaMP6s expression 7–10 days later. GCaMP6s expressing neurons were imaged using a two-photon laser scanning at 920 nm (Femto2D RC, Femtonics, Budapest, Hungary), equipped with a 16× Nikon water-immersion objective (0.8 NA). During imaging, mice were anesthetized with chlorprothixene (Sigma, C1671) (2.5 mg/kg) and maintained with 0.25% isoflurane. A Python-based user interface controlled visual stimulation, data recording and alignment. Layer 4 imaging was performed in steps of 20 μm, at depths of 300–440 μm below the pial surface. 250×350 pixel images were acquired at 6–10 Hz. Eyes were dilated with atropine 0.5% (Thea, 2094264) 15 min before imaging. Full-field, 100 ms NIR light was presented 5 times at each intensity to the contralateral eye. Detection of active cells was performed online as previously described (*21*) and subsequently refined and deconvolved offline (*24*). Trials with deconvolved calcium transients between 200–1500 ms after stimulus onset were considered responsive. Cells were considered responsive when at least 60% of trials were responsive for any light intensity. Normalized ΔF/F from raw fluorescence was calculated using the mean of fluorescent samples 150 ms before stimulus onset as the baseline. NIR responses were evaluated using a 3-sample average of the peri-stimulus activity. Peak responses within a 600 ms post-stimulus interval were extracted for every trial and averaged. To evaluate cortical wavelength preference, NIR stimulation was performed with wavelengths matched to and offset from nanorod absorption maxima. The same layer 4 population was imaged twice, once with 980 nm

stimulation of the eye and once with 915 nm stimulation. To establish response correspondence during wavelength preference experiments, imaging planes were manually aligned to image the same neurons across two conditions (matched and unmatched stimulation wavelengths). Wavelength preference index (WPI) was defined as:

$$WPI = (\Delta F/F_{980} - \Delta F/F_{915}) / (\Delta F/F_{980} + \Delta F/F_{915}).$$

Light intensity preference index was defined as:

$$LPI = (\Delta F/F_{\text{lower intensity}} - \Delta F/F_{\text{higher intensity}}) / (\Delta F/F_{\text{lower intensity}} + \Delta F/F_{\text{higher intensity}}).$$

Mouse behavior

Rd1 mice underwent surgery to attach a titanium headbar to the skull and were left to recover for 2–3 days before being placed on a water restriction schedule. Thereafter, mice were handled daily and received ~ 0.5–1 mL of water per session, until body weight reached ~ 80% of the *ad libitum* weight (typically within 5–7 days). Health status and weight were monitored daily. Before starting behavioral evaluation, mice were progressively habituated to the experimental setup, including head fixation and enclosure within a 'body' tube (*25*). Enclosure of the mouse body within a cylindrical acrylic tube was found to maximize animal comfort during head fixation. Eyes were dilated with atropine 0.5% 15 min before behavioral evaluation. Rd1 experiments were performed in the dark. NIR experiments in wild-type mice were performed in ambient light. Visible light experiments in wild-type mice were performed in the dark. Mice performed a voluntary action NIR detection task by licking a waterspout (blunt 18G needle, 5 mm from mouth) in response to full-field, 200 ms stimulation of one eye (915 nm, 980 nm, white light). Water (~7 μL) was automatically dispensed 500 ms after light onset, through a calibrated gravity water system gated with a solenoid pinch valve. NIR intensities were randomly interleaved. Inter-trial intervals ranged between 10–30 s. Training lasted 4 days for NIR light and/or 4 days for visible light. Typical sessions lasted ~ 40 min during which mice performed 80–100 trials. To assess the impact of the light cue, lick rates were calculated after stimulus onset but before water valve opening. Spontaneous background lick rates (1 s time window before stimulus onset) were subtracted from stimulus-driven lick rates. For Z scores, mean and standard deviation of a 500 ms background time interval were used. An Arduino Uno board provided control of the behavioral protocol, including lick detection, water valve opening, and variation of NIR stimulus intensities. Lick events were detected by a transistor-based circuit and recorded by a USB 6002 (National Instruments, Austin) data acquisition device. Custom control software was written in Python (SELS Software).

Two-photon calcium imaging in *ex vivo* human retina

OGB-1 calcium dye was bulk electroporated into human retinal explants as described above (see "Two-photon calcium imaging of mouse retinal ganglion cells"). Electroporation was observed to introduce OGB-1 into all 3 nuclear layers of the retina. Low melting temperature 1% agarose gel (Sigma, A2790) was added to the ganglion cell side to stabilize the retina and was kept in place throughout the experiment. Nanorods were added to the photoreceptor side (10^{10} nanorods). During activity monitoring, the human retina was continuously perfused with

Ames' solution bubbled with 95% O_2 and 5% CO_2 at ~37°C. For acousto-optic imaging, a z-stack was taken before NIR stimulation with the acousto-optic deflector two-photon (AOD) microscope (Femtonics, Budapest, Hungary) using a 16× water immersion objective (0.8 NA) to capture the 3D volume of the retina. Within this volume, the experimenter manually selected cell soma positions of OGB-1 filled cells. Full-field, 915 nm, 100 ms light stimulus was presented 5 times at each intensity. During stimulation the AOD scanned a set of square XY planes encompassing each cell body at ~50 Hz. Fluorescence values were analyzed offline by custom software in MATLAB. Neurons were segmented by selecting a cell center manually and applying Chan-Vese segmentation. NIR responses were evaluated using a 3-sample moving average of the peristimulus activity. Peak responses within an 800 ms post-stimulus interval were extracted for every trial and averaged. Cells were considered responsive when peak absolute fluorescence was > 4.5 standard deviations above the pre-stimulus fluorescence in at least 80% of trials.

Immunofluorescence and confocal imaging

HEK293T cells and retinas were fixed overnight in 4% paraformaldehyde and washed overnight with phosphate buffered saline (PBS) at 4°C. To improve antibody penetration, wholemount retinas were subjected to freeze-thaw cycles after cryoprotection with 30% sucrose. After washing in PBS, retinal wholemounts, 3% agarose-embedded (SeaKem, Lonza, 50004) 150 µm thick retinal vibratome sections (Leica VT1000 S) or HEK293T cells on coverslips were incubated for 2–4 h in blocking buffer containing 10% normal donkey serum (NDS, Chemicon), 1% BSA, 0.5% TritonX-100, and 0.01% sodium azide (Sigma) in PBS. Primary antibody treatment was performed for 5–7 days at room temperature in buffer containing 3% NDS, 1% BSA, 0.01% sodium azide, and 0.5% TritonX-100 in PBS. Primary antibodies used in this study were: rat monoclonal anti-GFP (Nacalai, 04404-84), rabbit polyclonal anti-GFP (Thermo Fisher Scientific, A11122), rabbit polyclonal anti-Cone Arrestin (Millipore, AB15282), rat monoclonal anti-RFP (Chromotek, 5F8-100), rabbit anti-RFP (Rockland, 600-401-379), goat polyclonal anti-Opsin mw/mw2/lw (Santa Cruz, sc22117), goat polyclonal anti-Opsin sw (Santa Cruz, sc14365), rabbit polyclonal anti-Capsaicin receptor (Millipore, AB5370), rat monoclonal anti-OLLAS (Novus Biologicals, NBP1-06713), mouse monoclonal anti-polyHis (Millipore, 05949), rabbit polyclonal anti-Iba1 (Genetex, GTX100042). Hoechst was used to stain cell nuclei. Apoptotic cells were detected using the *In Situ* Cell Death Detection Kit, Fluorescein (Roche, 11684795910). DNase I recombinant (Promega, M6101) digestion was used to induce DNA strand breaks in the positive control. For microscopy retinas were mounted on glass slides with ProLong Gold antifade reagent (Invitrogen, P36982). A Zeiss LSM 700 laser scanning confocal microscope was used to acquire images of antibody stained cells and tissues with an EC Plan-Neofluar 40×/1.30 oil M27 objective at up to 4 excitation laser lines according to secondary antibody specification. Expression was assessed from 1024×1024 pixel images in a z-stack with 0.75 µm steps. Images were processed using Imaris (Bitplane) and Image J (Fiji). AAV transduction was quantified from retinal wholemounts. In each sample the entire thickness of the retina was scanned by confocal microscopy at 3 or 5 randomly chosen areas in AAV transduced regions.

Transmission electron microscopy

To measure nanorod sizes 4 µL of nanorod stock solution was adsorbed for 2 min to glow-discharged formvar carbon-coated copper grids (Ted Pella Inc, Redding, USA, 01753-F). The

grids were then blotted and negatively stained on 2 droplets of 2% uranyl acetate solution (Electron Microscopy Sciences, 22400) for 20 s. Samples were imaged at a nominal magnification of 30000× using a Tecnai Spirit electron microscope (FEI, Eindhoven, Netherlands) operating at 120 kV. Electron micrographs were recorded using a bottom mount 4K×4K CCD FEI Eagle camera.

Scanning electron microscopy

Retinal samples were placed on glass slides. Nanorod stock solution was applied for 40 min at room temperature, followed by extensive rinses with deionized H_2O. The retina was dehydrated progressively for 30–50–70–90–95–100 (2×) and immersed in hexamethyldisilazane (Sigma, 440191) for 10 min (2×). Subsequently, the samples were dried for 90 min at 60°C. Samples were metalized with gold palladium (Quorum, SC7620) for 15 s and imaged in a scanning electron microscope (FEI Versa 3D) at 5 kV and 3 nm per pixel with an ETD detector. Lookup tables were inverted in post-processing.

Statistical Analysis

We used the following statistical tests: Mann-Whitney U test (two-tailed) and Wilcoxon Matched-Pairs Signed Rank Test. P values are stated in the text and in Table S1. n.s refers to $P \geq 0.05$. In all figures; boxplots: center line, median; box edges, first and third quartiles; whiskers, 10^{th} and 90^{th} percentile.

Safety

NIR exposures are governed by ocular laser safety standards (ANSI Z136.1-2000). We calculated maximum permissible exposures according to ANSI-Z136.1 (*26*). Maximum permissible radiant power ($MP\Phi$) which may be chronically delivered to the retina is:

$$MP\Phi = 6.93\times10^{-5}\, C_T\, C_E\, P^{-1}$$

where $C_T = 10^{0.002(\lambda[nm]-700)}$ in the 700 - 1050 nm range, with $C_T = 2.7$ at λ = 915 nm and $C_T = 3.6$ at λ = 980 nm. C_E depends on the angular spread of the incident beam and for retinal spot sizes greater than 1.7 mm in diameter, $\alpha = \alpha_{max} = 100$ mrad and $C_E = 6.67\times10^{-3}\ \alpha^2 = 66.7$ W (*26*). P is the pupil size factor, P = 1 for NIR wavelengths. Maximum permissible exposure for 915 nm light is 0.0125 Watts (12.5 mW). Maximum permissible exposure for 980 nm light is 0.0166 Watts (16.6 mW). In Maxwellian ophthalmic illumination the maximum permissible retinal radiant exposure MPH_r is given by the power entering the pupil Φ divided by the retinal exposure area. For $\alpha = \alpha_{max} = 100$ mrad the dimension of the exposed retina is assumed to be 1.7 mm in diameter. Thus for chronic exposure $MPH_r = 5.5$ mW mm^{-2} (5500 W m^{-2}) for 915 nm and MPH_r = 7.3 mW mm^{-2} (7300 W m^{-2}) for 980 nm. rTRPV1 activation *in vivo* requires 4060 W m^{-2} of NIR 915 nm light (Table S4). sTRPA1 activation *in vivo* requires 1840 W m^{-2} of NIR 915 nm light (Table S4). Both intensities are below ocular safety limits for NIR 915 nm light.

To assess thermal aspects, we calculated temperatures at the nanorod. We assumed a monolayer of gold nanorods equally spaced. We calculated nanorod absorption cross-sections from measured optical densities and number of nanorods in the eye. Mouse eye optical properties were assumed

to be similar to water, absorption coefficient = 6.6×10^{-6} μm^{-1} at 915 nm, except for pigmented tissues. Absorption coefficient for pigmented tissue was taken as 0.2 mm^{-1}. We then solved the 1D heat differential equation:

$$Q = (\kappa T^{(0,1)}[x, t] / \alpha) - \kappa T^{(2,0)}[x, t]$$

where Q is heat flux, κ is thermal conductivity, α is thermal diffusivity, x is distance, t is time and T is temperature. Mouse eye thermal properties were assumed to be similar to water, with thermal diffusivity = 150.87 $\mu m^2/ms$, thermal conductivity = 6.26×10^{-4} kg $\mu m/(ms^3K)$, mass density = 9.93×10^{-16} $kg/\mu m^3$. For TRPV1, nanorod temperatures reach a maximum of 43.0°C. For TRPA1, nanorod temperatures reach a maximum of 39.7°C. Published reports of TRPV1 and TRPA1 thermosensitivity report activation temperatures of ~43°C for TRPV1 and ~39°C for TRPA1 (*3, 27*).

Supplementary Text

Near-infrared light stimulation

For human patients with retinal degeneration visual patterns can be projected onto the retina by biomimetic eye goggles (https://www.gensight-biologics.com, Medical Device GS030; Clinical Trials ID: NCT03326336). The device consists of an external camera, a signal processing unit and a high-brightness, near-to-eye display that is NIR light compatible. Light patterns are projected by micromirror arrays. In this way, natural scenes are converted to modified NIR images. A device with similar properties but small enough to fit a mouse eye is currently not available. In addition, NIR LEDs positioned in the environment are not bright enough to activate TRP channels. It was therefore not possible to present structured NIR stimuli or perform behavioral tests with freely moving animals.

Compatibility with remaining vision

To prevent superimposition of visible and NIR responses in light sensitive retinal regions, two solutions may be considered. First, in conventional human subretinal surgery, the procedure is a vitrectomy followed by formation of a subretinal bleb. Since bleb formation involves separation of tightly apposed photoreceptor and retinal pigment epithelial layers, blebs have defined perimeters, which spatially restrict virus and nanorod deposition to specific, pre-determined sites. Central retina (macula) may be transduced while peripheral retinal regions remain unmodified. Second, NIR vision requires NIR images to be projected by stimulator eye goggles into the patient eye. Images can be focused onto the macula via an eye tracker based projection system. In nearby regions NIR intensities would be reduced by the inverse square law. Since lower NIR intensities do not generate enough heat to activate TRP channels, unfocussed NIR light is unlikely to lead to activation.

Nanorod stability *in vivo*

Cytotoxicity studies report low or no toxicity of nanorods up to 70 days post intravitreal or subretinal injection (*28-33*). Longer-term effects in the eye are not yet known. Stable, covalent polymer bridges bind antibodies to nanorods. Antibody-epitope binding relies on weaker, non-covalent bonds. Gold nanoparticle stability (plasmon band, hydrodynamic diameter, core diameter) ranges from highly-stable to ultra-stable (*34-38*). Ultra-stable gold nanoparticles maintain stability in various environments including solubilization in ionic media, freeze-drying, heating (65°C), ultracentrifugation and autoclave sterilization (*39-40*). Preclinical studies will be required to determine stability precisely.

Nanorod tuning

We tuned responses to different wavelengths for several reasons. First, enabling light sensitivity in a blind human retina requires eye goggles that utilize specific wavelengths. Compatibility with current and future NIR projector goggles requires tunable NIR detectors. Second, over time it may be found that some NIR wavelengths are better tolerated by patients than others. It is then advantageous to know that nanorod manufacturing technologies can be exploited to tune responses

to different wavelengths, if required. Third, if it is possible to segregate nanorods by type around cone photoreceptors, in the future this could be used for inducing color vision. Fourth, since maximum permissible radiant exposures vary with incident wavelength, tuning responses to different NIR wavelengths plays an important role in compliance with safety standards.

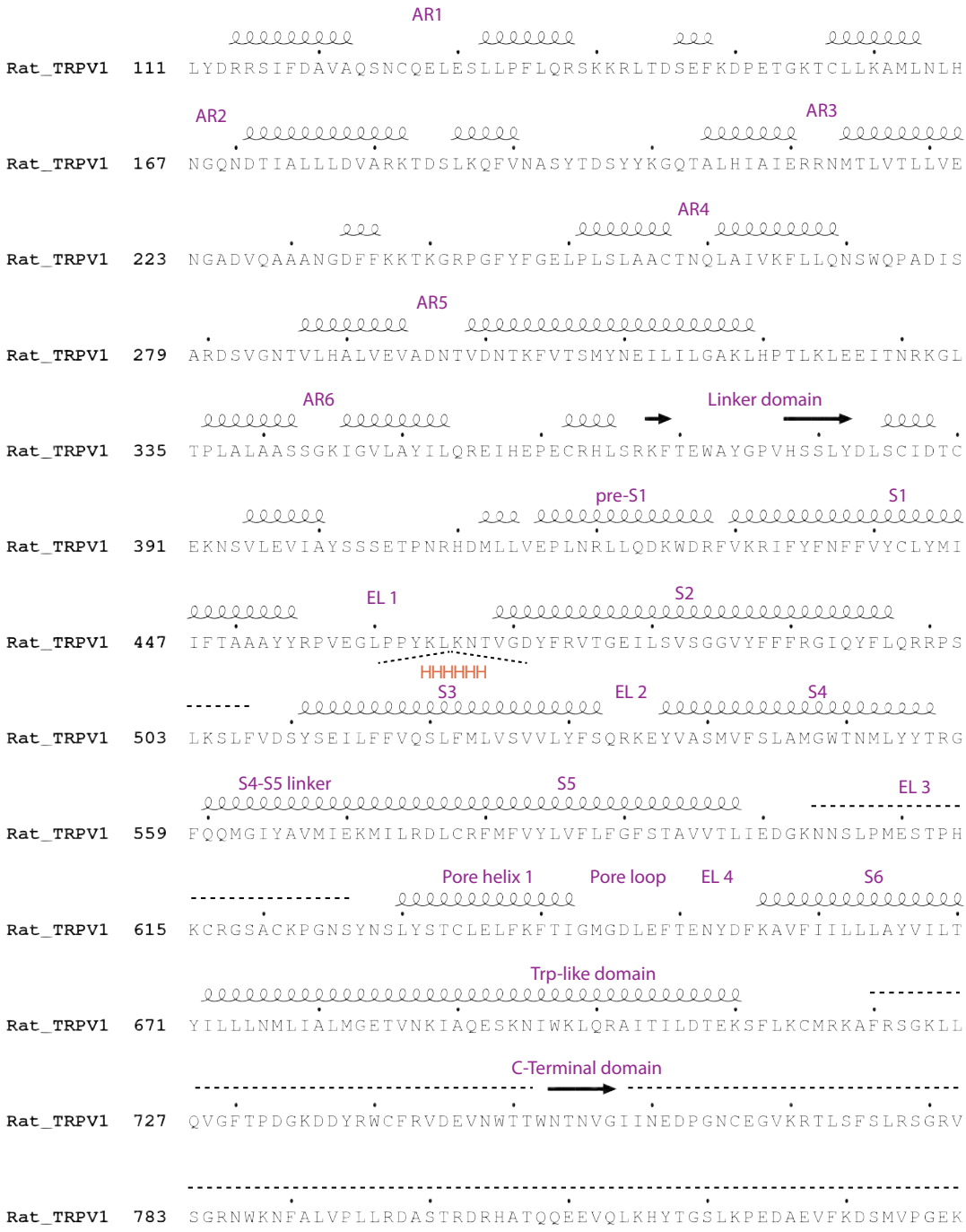

Fig. S1. Peptide sequence of rat TRPV1, starting at amino acid 111. 6x-His (HHHHHH) epitope tag insertion at amino acid 465 (EL1) is highlighted with tilted dashed lines. Secondary structure elements are indicated above the sequence as spirals (helices) and arrows (β strands). Regions with no assigned secondary structure are indicated by horizontal dashed lines. Black dots mark the position of every tenth amino acid. EL refers to extracellular loop, AR to ankyrin repeat, S to transmembrane domain.

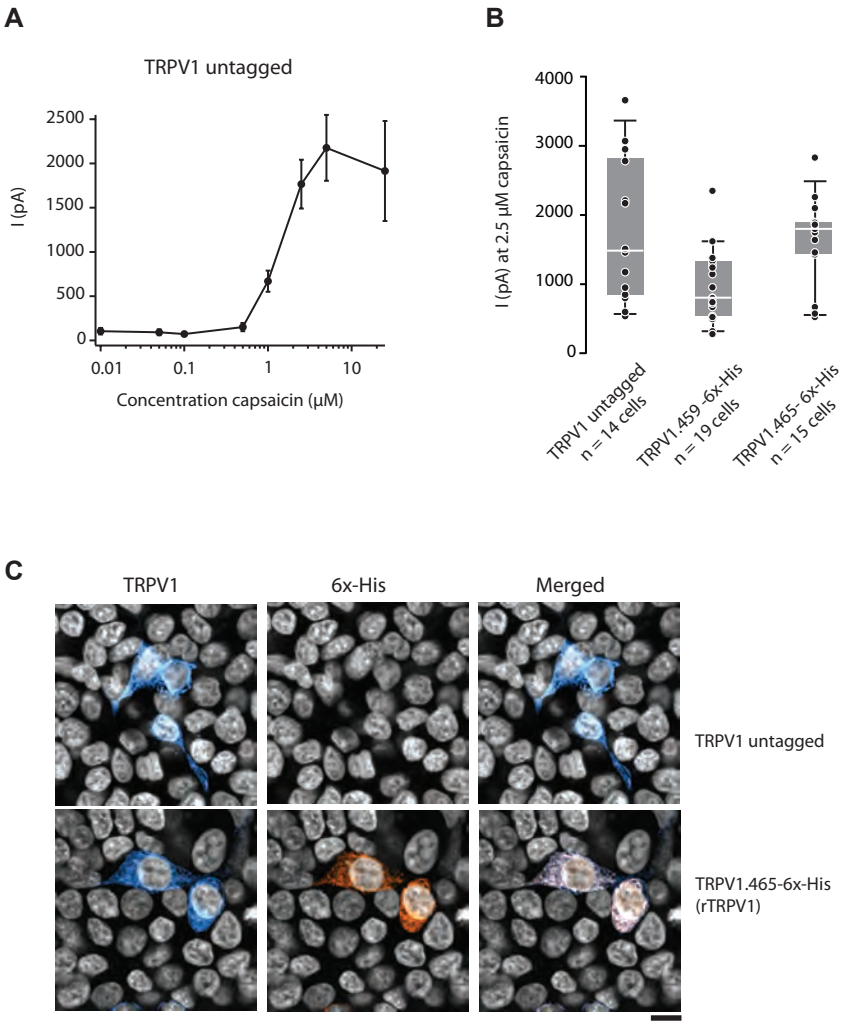

Fig. S2. Capsaicin-evoked whole-cell currents in HEK293T cells expressing rat TRPV1 channel variants. **(A)** Capsaicin dose-response curve for untagged rat TRPV1. Error bars, s.e.m. **(B)** Comparison of untagged TRPV1 with tagged variants at 2.5 μM capsaicin. **(C)** Top row, top views of HEK293T cells transduced with untagged TRPV1, immunostained for TRPV1 (left, blue), 6x-His (middle, orange), and merging the two (right). Grey, Hoechst nuclear stain. Bottom row, same views for HEK293T cells transduced with TRPV1.465-6x-His (rTRPV1). Scale bar 10 μm.

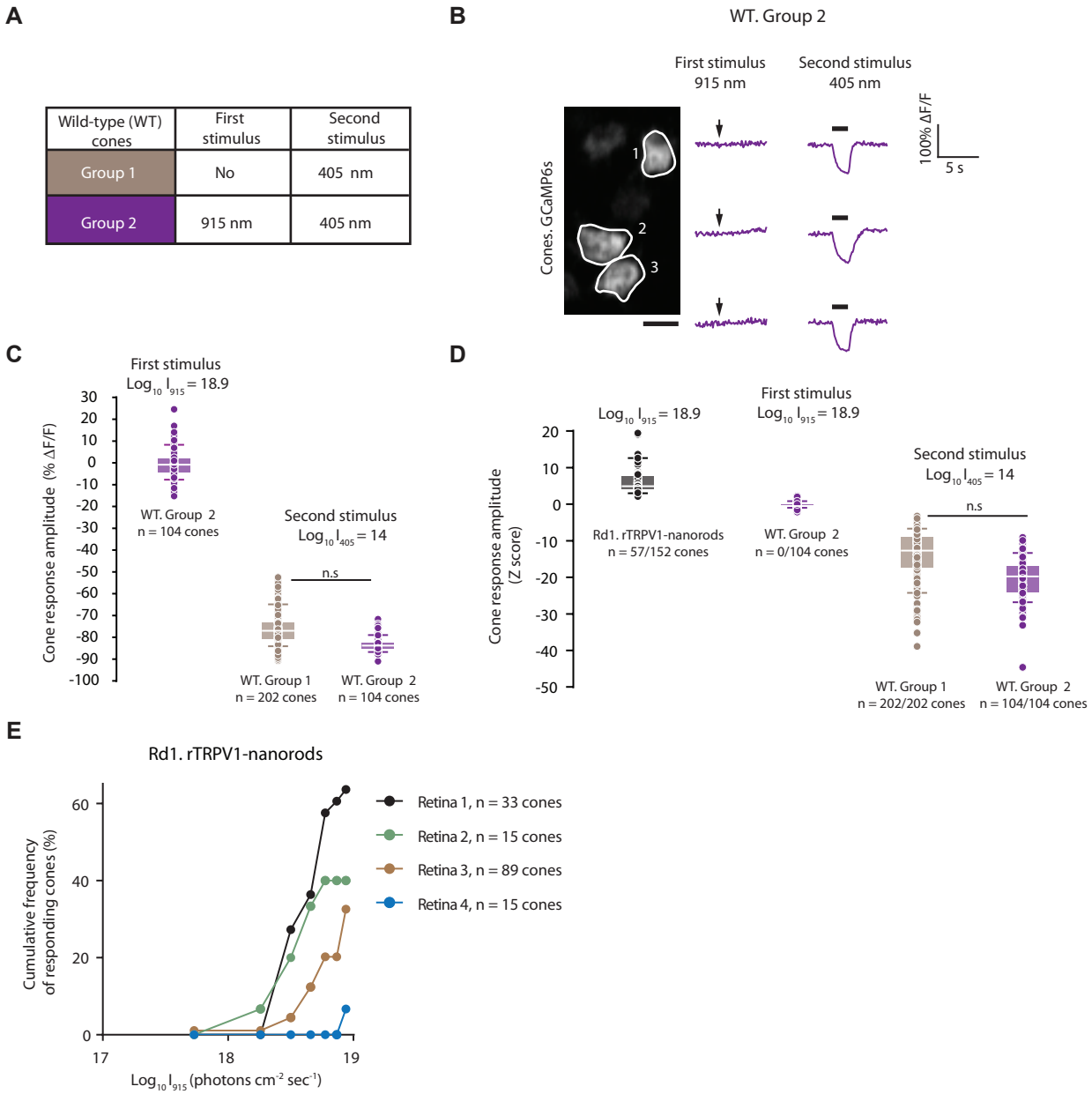

Fig. S3. Near-infrared and visible light responses in mouse cone photoreceptors. **(A)** Wild-type (WT) cone experiments. Group 1 (brown, $n = 3$ mice), visible light only. Group 2 (purple, $n = 3$ mice), first NIR then visible light. **(B)** Example calcium responses (mean ΔF/F, 3 repetitions) recorded from cone axon terminals in WT retinas. Stimulus, full-field. Left, 915 nm, $\log_{10}$ light intensity = 18.9. Right, 405 nm, $\log_{10}$ light intensity =14. Black bars (2 s) and arrows (100 ms), stimulus timing. Two-photon images of GCaMP6s-expressing cone axon terminals (white circles), left of the response curves. Scale bar 5 µm. **(C)** WT cone response amplitudes (ΔF/F) for Group 1 and 2. Note that two-photon functional imaging may lead to NIR light adaptation in wild-type cones, which may then not show strong responses to additional NIR light stimulation. **(D)** Rd1 (n = 4 mice) and WT (Group 1 and 2) cone response amplitudes (Z score). Rd1 cones transduced with rTRPV1 and nanorods (λ_{abs} = 915 nm). Note that due to low baseline fluorescence, rd1 cone responses were recorded with higher PMT gain, leading to lower Z scores in rTRPV1-nanorod injected rd1 retinas compared to wild-type retinas. x/y cones refers to x responding cones of the y measured. Cones were considered responding when absolute Z score values exceeded 1.5 for each stimulus repetition. **(E)** Cumulative frequency of responding rTRPV1 transduced rd1 cones with nanorods (λ_{abs} = 915 nm) for single retinas.

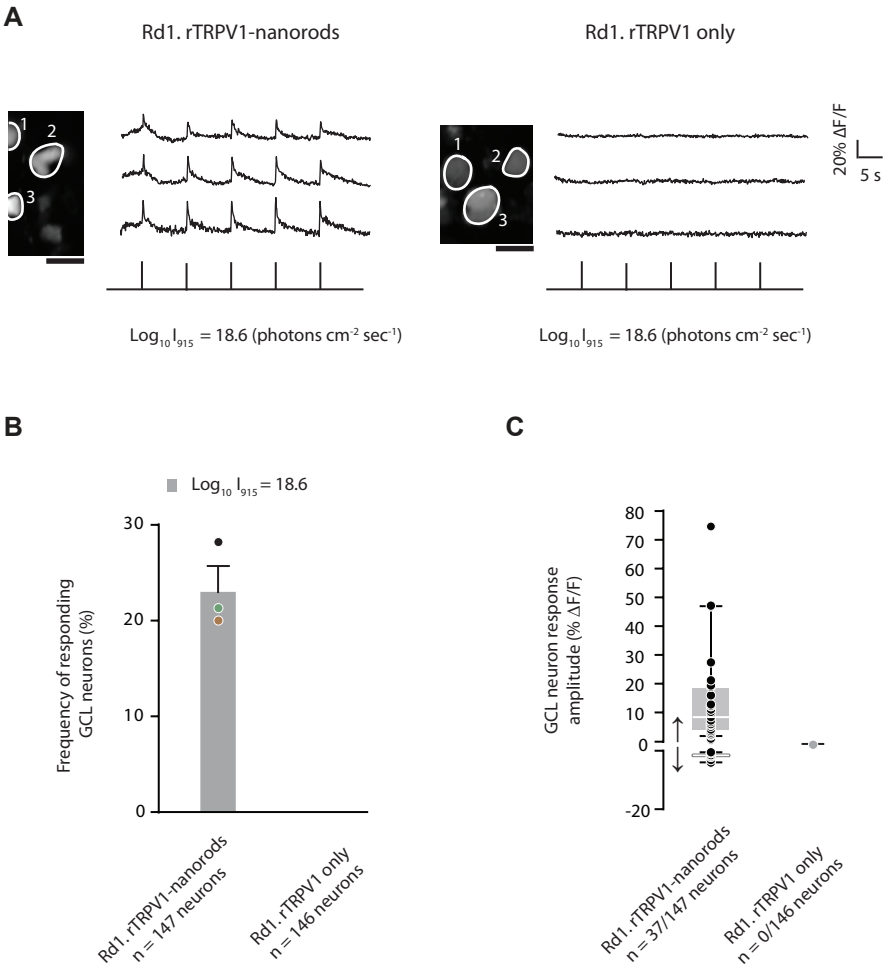

Fig. S4. Near-infrared light responses in neurons of the mouse retinal ganglion cell layer (GCL). **(A)** Example calcium responses (mean ΔF/F, 5 repetitions) recorded from GCL neurons in P69-P72 rTRPV1-nanorods (left) and rTRPV1 only (right) transduced rd1 retinas in response to full-field NIR light. Vertical lines at bottom, stimulus (915 nm, 100 ms) timing. Two-photon images of Oregon Green BAPTA-1 (OGB-1) filled cell bodies (white circles), left of the response curves. Scale bar 20 μm. **(B)** Frequency of responding GCL neurons in retinas transduced with both rTRPV1 and nanorods (λ_{abs} = 915 nm, *n* = 3 mice) or with rTRPV1 only (*n* = 3 mice). Each data point (colored black, green, brown) represents the response of a single retina. **(C)** GCL neuron response amplitudes (ΔF/F) at $\log_{10}$ light intensity = 18.6. Increase (↑) and decrease (↓) of calcium signal are shown separately. x/y neurons refers to x responding GCL neurons of the y measured.

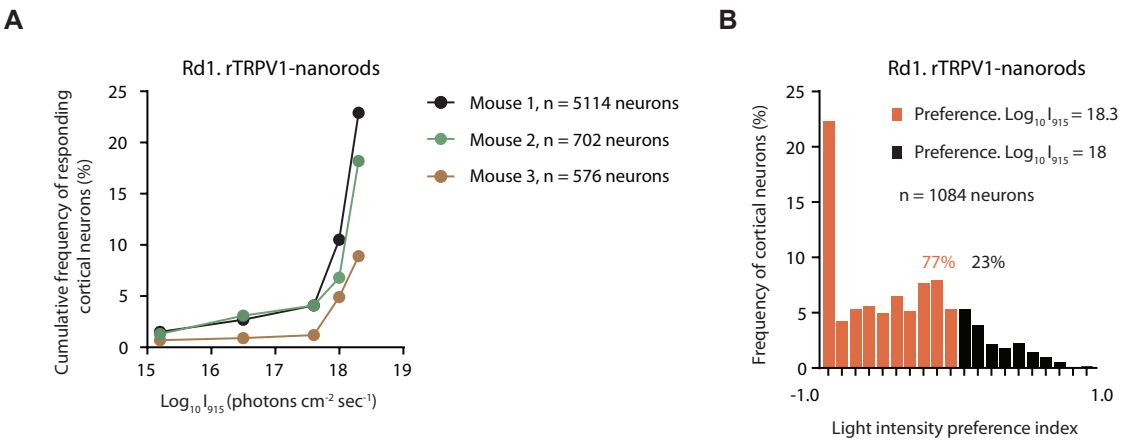

Fig. S5. Near-infrared light responses in mouse primary visual cortex. **(A)** Cumulative frequency of responding cortical neurons in individual P51-P83 rd1 mice transduced with both rTRPV1 and nanorods (λ_{abs} = 915 nm). **(B)** Frequency of cortical neurons as a function of the light intensity preference index (LPI) in mice transduced with rTRPV1 and nanorods (λ_{abs} = 915 nm, n = 3 mice). Larger fraction (orange, LPI < 0, 77%) of neurons prefer higher intensity light ($\log_{10}$ light intensity = 18.3) over lower intensity light ($\log_{10}$ light intensity = 18) (black, LPI > 0, 23%).

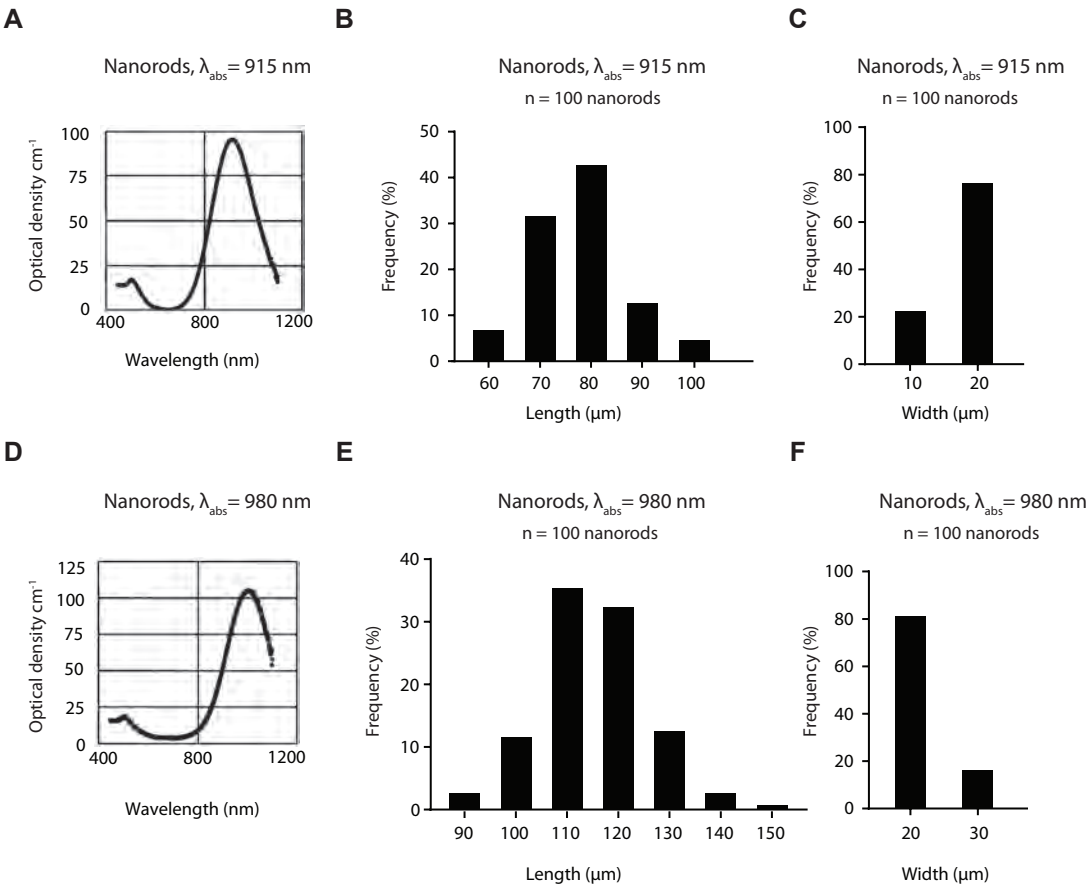

Fig. S6. Nanorod properties. **(A)** Optical density of gold nanorods tuned to 915 nm. **(B, C)** Histograms of length (B) and width (C) distributions giving rise to optical density in (A). **(D)** Optical density of gold nanorods tuned to 980 nm. **(E, F)** Histograms of length (E) and width (F) distributions giving rise to optical density in (D).

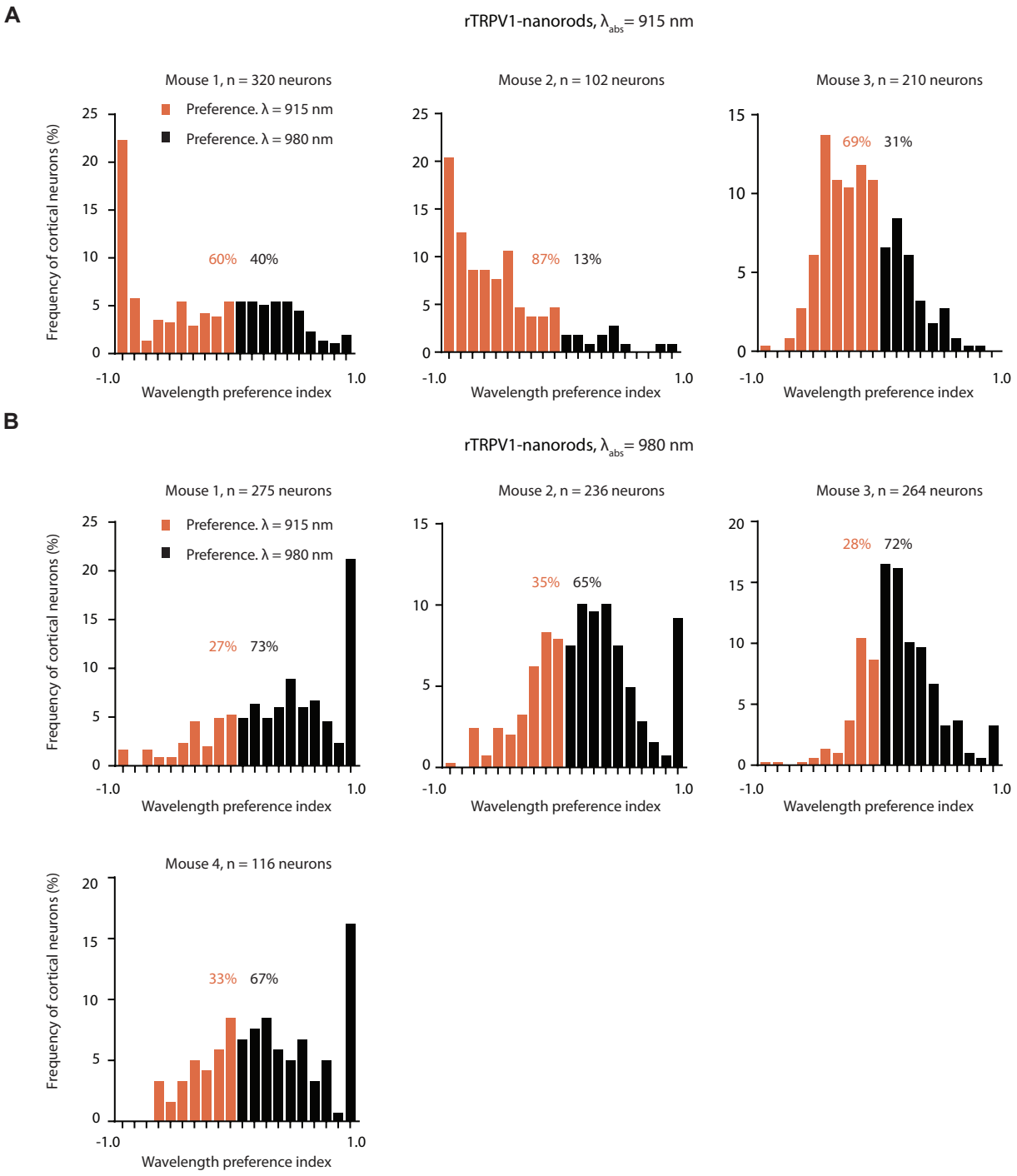

Fig. S7. Near-infrared light responses in mouse primary visual cortex. **(A)** Frequency of cortical neurons as a function of the wavelength preference index (WPI) in mice transduced with rTRPV1 and nanorods with λ_{abs} = 915 nm for individual animals. Log_{10} light intensity = 18.3. Larger fraction of 915 nm (WPI < 0) over 980 nm (WPI > 0) light preferring neurons. **(B)** Frequency of cortical neurons as a function of the wavelength preference index (WPI) in mice transduced with rTRPV1 and nanorods with λ_{abs} = 980 nm for individual animals. Log_{10} light intensity = 18.3. Larger fraction of 980 nm (WPI > 0) over 915 nm (WPI < 0) light preferring neurons. Experiments performed in P51-P71 rd1 mice.

Fig. S8. Pairwise sequence alignment between C-terminal domains of human and snake TRPA1. Ollas epitope tag insertions at amino acid 755 (EL1) and 824 (EL2) are highlighted with tilted dashed lines and the tag sequence is indicated. White text marks identical amino acid residues. Red text marks similar amino acid residues. Secondary structure elements of human TRPA1 are indicated above the sequence as spirals (helices). Regions with no assigned secondary structure are indicated by horizontal dashed lines. Black dots mark the position of every tenth amino acid of human TRPA1. EL refers to extracellular loop, AR to ankyrin repeat, S to transmembrane domain.

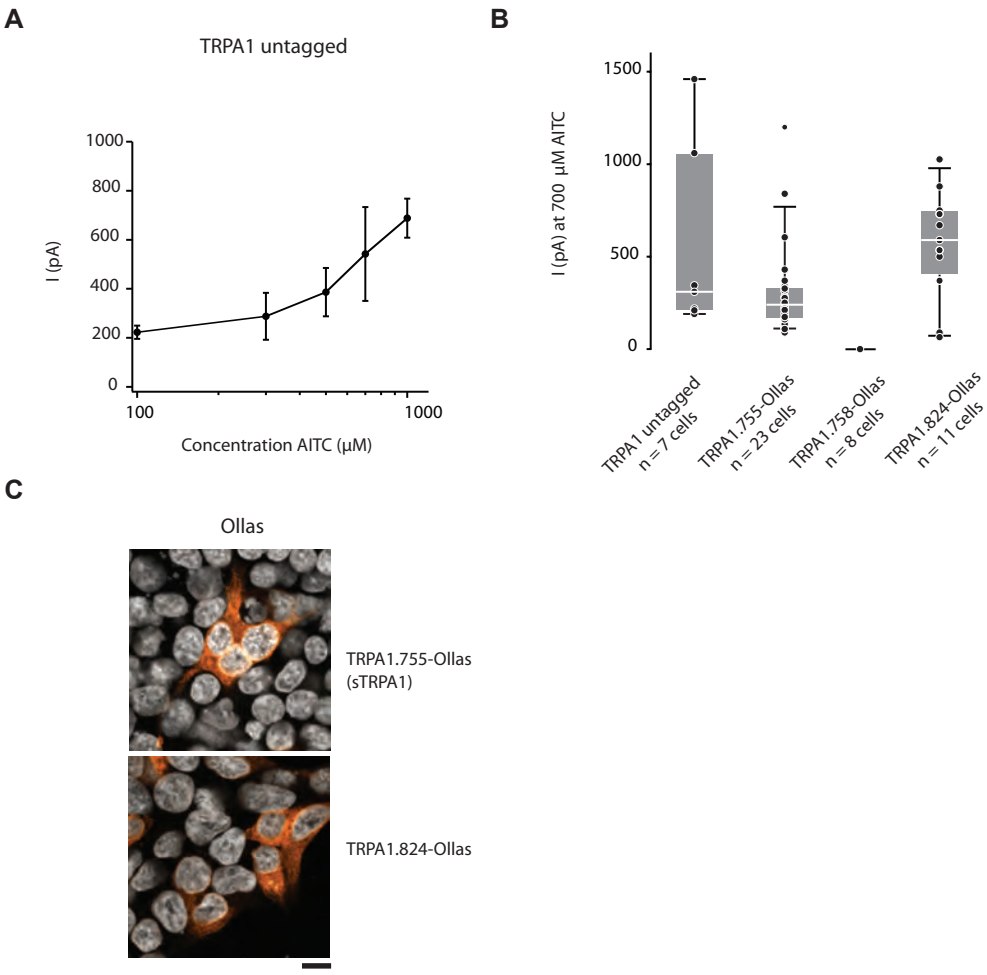

Fig. S9. Allyl isothiocyanate (AITC)-evoked whole-cell currents in HEK293T cells expressing snake TRPA1 channel variants. **(A)** AITC dose-response curve for untagged snake TRPA1. Error bars, s.e.m. **(B)** Comparison of untagged TRPA1 with tagged variants at 700 μM AITC. **(C)** Top, top views of HEK293T cells transduced with TRPA1.755-Ollas (sTRPA1), immunostained for Ollas (orange). Bottom, same views for HEK293T cells transduced with TRPA1.824-Ollas. Grey, Hoechst nuclear stain. Scale bar 10 μm.

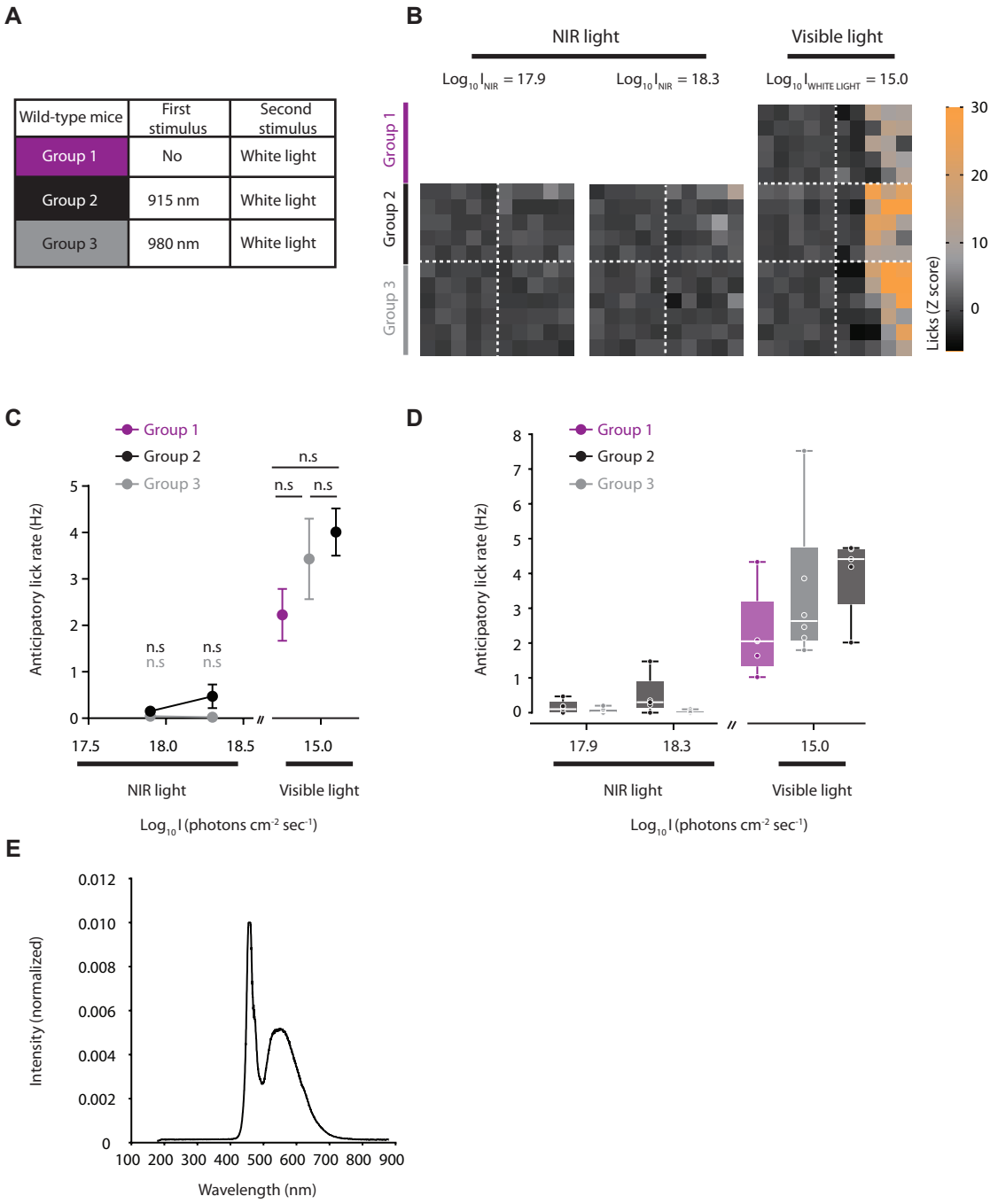

Fig. S10. Light guided wild-type mouse behavior. **(A)** Group 1 (purple, $n = 5$ mice), visible light stimulation only. Group 2 (black, $n = 5$ mice), NIR 915 nm and visible light stimulation. Group 3 (grey, $n = 6$ mice), NIR 980 nm and visible light stimulation. Full-field stimulation of one eye (200 ms) cues water presentation for head-fixed, water-restricted animals. Mice respond by licking before (anticipation) or after the appearance of water. **(B)** Lick response heat maps. Rows, responses of different mice. Columns, responses in 100 ms time bins. Responses shown separately for Group 1, 2 and 3. Left, stimulus $\log_{10}$ light intensity = 17.9. Middle, stimulus $\log_{10}$ light intensity = 18.3. Right, stimulus $\log_{10}$ light intensity = 15.0 **(C)** Mean anticipatory lick rates quantified from (B) as a function of light intensity. Error bars, s.e.m. **(D)** Anticipatory lick rates from (C) for single animals. **(E)** Spectral composition of white light used in mouse behavior experiments, normalized to yield an area of one under the curve.

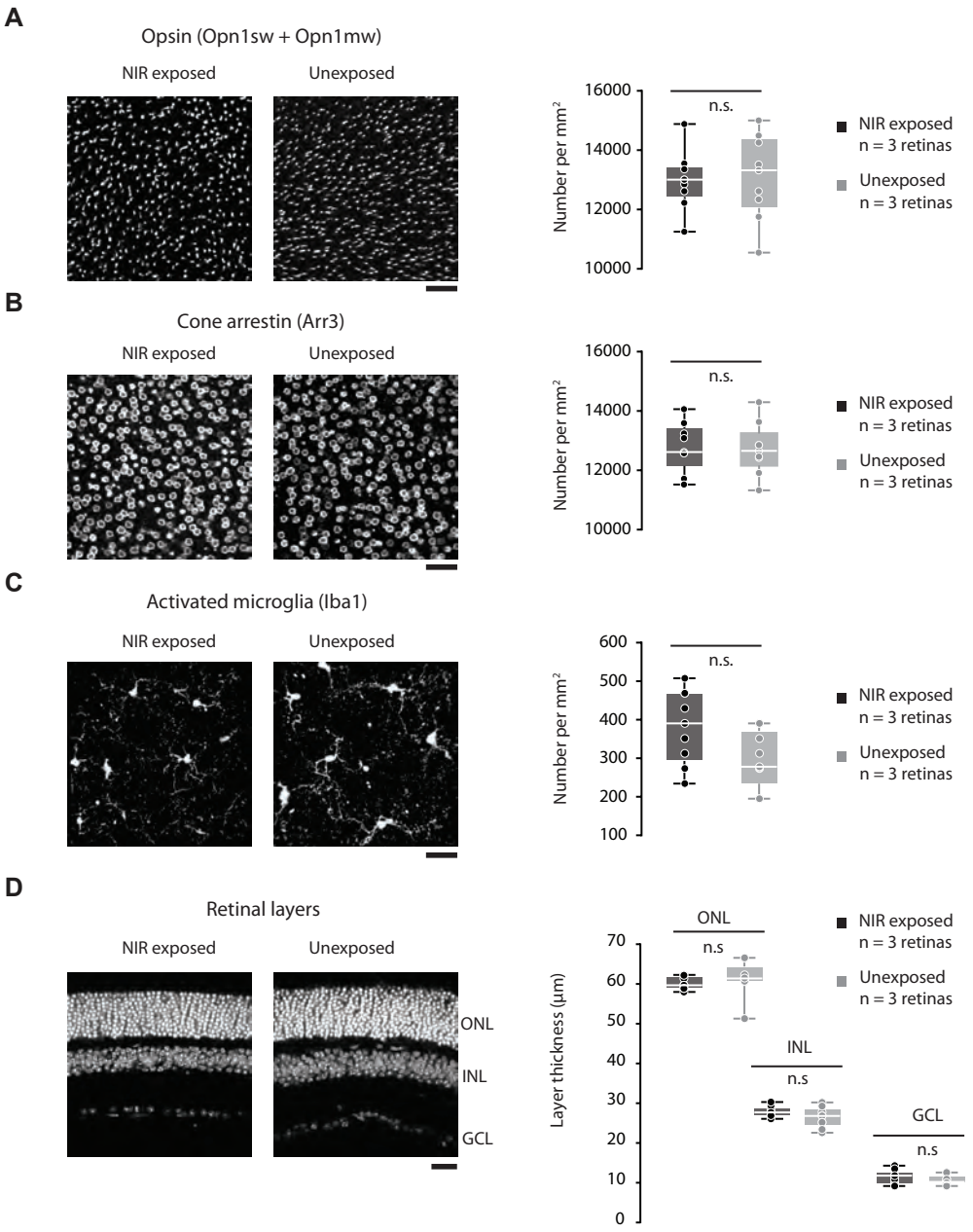

Fig. S11. Safety of prolonged near-infrared light exposure in the mouse retina. **(A, B, C)** Left, top views of wild-type retinas exposed to NIR light (915 nm) during behavioral training (n = 3 mice). Middle, top views of control, unexposed wild-type retinas (n = 3 mice). Right, number of immunostained cells per mm^2 in wild-type retinas exposed to NIR light (black) and control, unexposed wild-type retinas (grey). **(A)** Immunostained for short wavelength (sw) and medium wavelength (mw) Opsin (white). **(B)** Immunostained for cone photoreceptor marker, Cone arrestin (white). **(C)** Immunostained for activated microglia marker, Iba1 (white). **(D)** Cross-sections of NIR light exposed (left, n = 3 mice) and control, unexposed (middle, n = 3 mice) wild-type retinas. White, Hoechst nuclear stain. Right, thickness of retinal layers in wild-type retinas exposed to NIR light (black) and control, unexposed wild-type retinas (grey). ONL, outer nuclear layer; INL, inner nuclear layer; GCL, ganglion cell layer. In all microscopy panels, scale bars = 25 µm. In all quantification panels, each data point is collected from a different region of a retina (3 per retina).

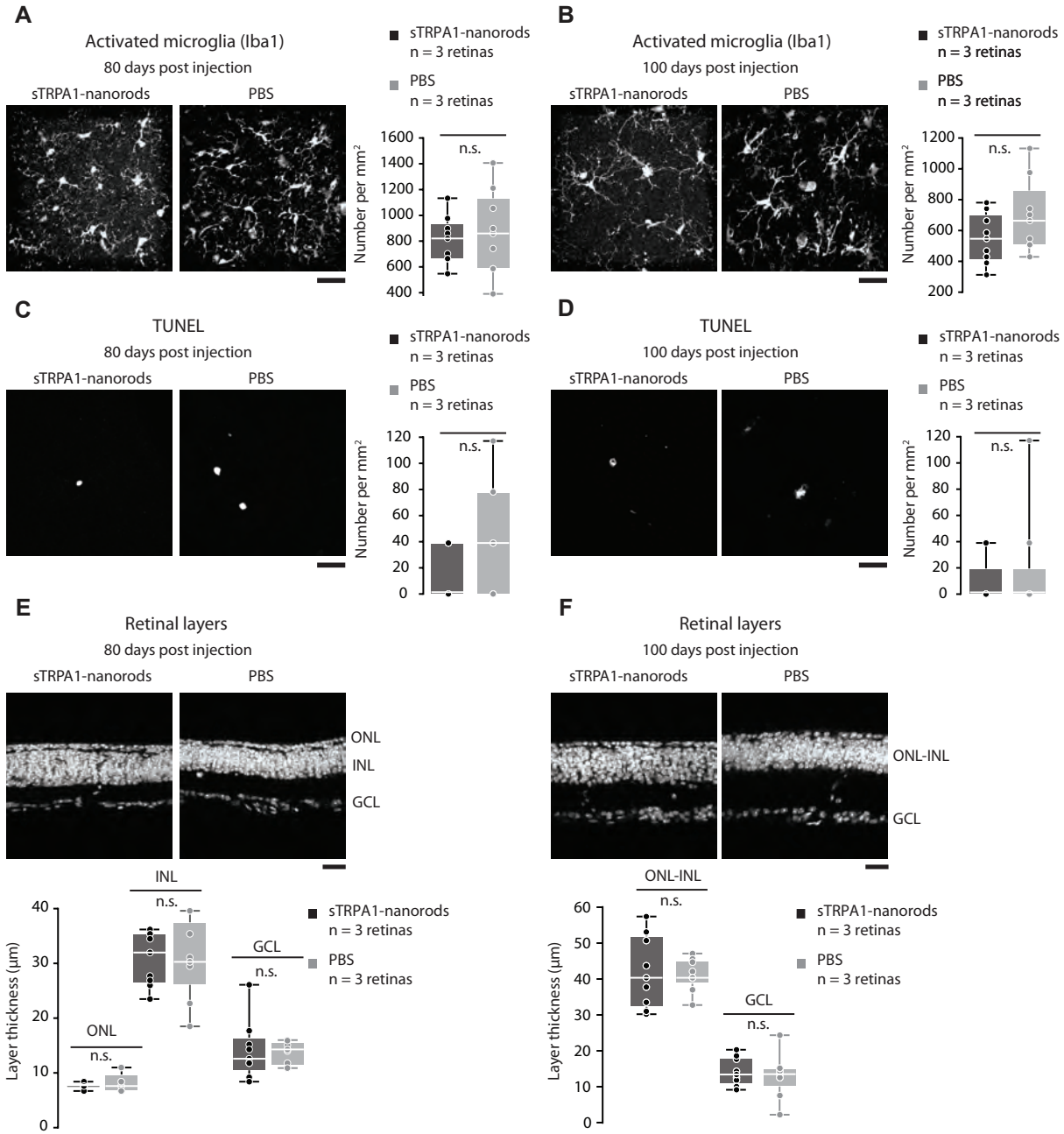

Fig. S12. Safety of intraocular sTRPA1-nanorods injection in the mouse retina. **(A-D)** Left, top views of rd1 retinas injected with sTRPA1-nanorods at P30 (n = 3 mice). Middle, top views of control rd1 retinas injected with PBS at P30 (n = 3 mice). Right, number of detected cells per mm^2 in rd1 retinas injected with sTRPA1-nanorods (black) and control, PBS injected rd1 retinas (grey). **(A, B)** Immunostained for activated microglia marker, Iba1 (white) 80 (A) and 100 days (B) post injection. **(B, C)** TUNEL apoptosis assay (white) 80 (C) and 100 days (D) post injection. **(E, F)** Left top, cross-sections of rd1 retinas injected with sTRPA1-nanorods at P30 (n = 3 mice). Right top, cross-sections of control rd1 retinas injected with PBS at P30 (n = 3 mice). White, Hoechst nuclear stain. Bottom, thickness of retinal layers in rd1 retinas injected with sTRPA1-nanorods at P30 (black) and control rd1 retinas injected with PBS at P30. ONL, outer nuclear layer; INL, inner nuclear layer; GCL, ganglion cell layer. **(E)** 80 days post injection. **(F)** 100 days post injection, when ONL and INL converge. In all microscopy panels, scale bars = 25 µm. In all quantification panels, each data point is collected from a different region of a retina (3 per retina).

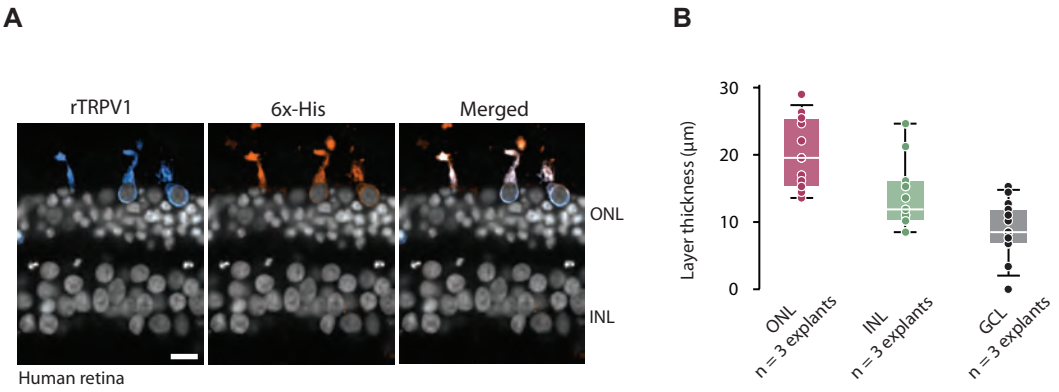

Fig. S13. Expression of rTRPV1 in photoreceptors of the *ex vivo* human retina. **(A)** Cross-sections of human retina transduced with both rTRPV1 and nanorods, immunostained for TRPV1 (left, blue), 6x-His (middle, orange), and merging the two (right). Grey, Hoechst nuclear stain. Scale bar 10 µm. **(B)** Retinal layer thickness at eight weeks post-mortem. Each data point is collected from a different region of a retinal explant (5 regions per explant). ONL, outer nuclear layer; INL, inner nuclear layer; GCL, ganglion cell layer.

	Quantification
A	Mann-Whitney U test, P = 0.86; TRPV1.465-6x-His, 1633 ± 164 pA, n = 15 cells; TRPV1, 1766 ± 276 pA, n = 14 cells; mean ± s.e.m
B	Mann-Whitney U test, P = 0.021; TRPV1.459-6x-His, 976 ± 118 pA, n = 19 cells; mean ± s.e.m
C	55 ± 10%, mean ± s.d*;* n = 12813 cones per mm^2 (*10*), n = 7042 TRPV1 positive cones per mm^2
D	98 ± 1.6%, mean ± s.d; n = 7216 TRPV1 positive cells per mm^2, n = 7042 TRPV1 positive cones per mm^2
E	Mann-Whitney U test, P = 0.71; n = 7042 TRPV1 positive cones per mm^2, n = 6820 6x-His positive cones per mm^2
F	Mann-Whitney U Test, P = 0.057; ΔF/F; rTRPV1-nanorods, 325 ± 59%, n = 4 mice; WT, 75 ± 0.5%, n = 3 mice; mean ± s.e.m
G	Z score; rTRPV1-nanorods, 6.2 (2.1-19.5), n = 4 mice; WT, 14 (3.1-38.9), n = 3 mice; mean (range)
H	Mann-Whitney U Test, P = 0.036; rTRPV1-nanorods, 21.1%, n = 3 mice; control, 3.1%, n = 5 mice
I	Wilcoxon Matched-Pairs Signed Rank Test, P = 0.031; 70% of neurons with WPI > 0, n = 4 mice
J	Wilcoxon Matched-Pairs Signed Rank Test, P = 0.031; 67% of neurons with WPI < 0, n = 3 mice
K	Mann-Whitney U test, P = 0.22; TRPA1.755-Ollas, 315 ± 56 pA, n = 23 cells; TRPA1, 542 ± 192 pA, n = 7 cells; mean ± s.e.m
L	Mann-Whitney U test, P = 0.52; TRPA1.824-Ollas, 566 ± 83 pA, n = 11 cells; mean ± s.e.m
M	50 ± 13%, mean ± s.d*;* n = 12813 cones per mm^2 (*10*), n = 6362 Ollas positive cones per mm^2
N	99 ± 0.8%, mean ± s.d*;* n = 6403 Ollas positive cells per mm^2, n = 6362 Ollas positive cones per mm^2
O	Mann-Whitney U test, P = 0.70; rTRPV1-nanorods, 0.17 ± 0.12 Hz, n = 9 mice; control, 0.043 ± 0.02 Hz, n = 10 mice; mean ± s.e.m
P	Mann-Whitney U test, P = 0.019; sTRPA1-nanorods, 0.75 ± 0.31 Hz, n = 9 mice; mean ± s.e.m
Q	Mann-Whitney U test, P = 0.001; rTRPV1-nanorods, 1.7 ± 0.34 Hz, n = 9 mice; control, 0.11 ± 0.057 Hz, n = 10 mice; mean ± s.e.m
R	Mann-Whitney U test, P = 0.019; sTRPA1-nanorods, 3.4 ± 0.64 Hz, n = 9 mice; mean ± s.e.m
S	Mann-Whitney U test, P = 0.19; sTRPA1-nanorods, 3.4 ± 0.64 Hz, n = 9 mice; wild-type group 1, 2.2 ± 0.56 Hz, n = 5 mice; mean ± s.e.m
T	Mann-Whitney U test, P = 0.52; rTRPV1-nanorods, 1.7 ± 0.34 Hz, n = 9 mice; wild-type group 1, 2.2 ± 0.56 Hz, n = 5 mice; mean ± s.e.m
U	94.5 ± 4.2%, mean ± s.d*;* n = 2583 rTRPV1 positive cells per mm^2, n = 2477 rTRPV1 positive photoreceptors per mm^2

Table S1. Details of quantification and statistical tests.

Nanorod properties	**Nanorods λ_{abs} = 915 nm Anti-6x-His**	**Nanorods λ_{abs} = 980 nm Anti-6x-His**	**Nanorods λ_{abs} = 915 nm Anti-Ollas**
Surface plasmon resonance (nm)	905–915	980–990	903–915
Concentration (nanorods per mL)	10^{13}	10^{13}	10^{13}
IgG (per nanorod)	18–22	24–25	19–20
pH	7	7	7
Solution	PBS	PBS	PBS
Zeta Potential (mV)	-18	-15	-16

Table S2. Nanorod properties.

Plasmids generated	TRP origin	Promoter	Experiment
pAAV-EF1a-TRPV1-T2A-GFP	rat	EF1a	HEK293T
pAAV-EF1a-TRPV1.459-6x-His-T2A-mCherry	rat	EF1a	HEK293T
pAAV-EF1a-TRPV1.465-6x-His-T2A-mCherry	rat	EF1a	HEK293T
pAAV-EF1a-TRPA1-T2A-GFP	snake	EF1a	HEK293T
pAAV-EF1a-TRPA1.755-Ollas-T2A-mCherry	snake	EF1a	HEK293T
pAAV-EF1a-TRPA1.758-Ollas-T2A-mCherry	snake	EF1a	HEK293T
pAAV-EF1a-TRPA1.824-Ollas-T2A-mCherry	snake	EF1a	HEK293T
pAAV-mCar-TRPV1.465-6x-His (rTRPV1)	rat	mCar	Mouse
pAAV-mCar-TRPA1.755-Ollas (sTRPA1)	snake	mCar	Mouse
pAAV-CAG-TRPV1.465-6x-His	rat	CAG	Human

Table S3. TRP plasmid list. mCar refers to photoreceptor specific mouse cone arrestin promoter.

Experiment	**I_{915}** (photons cm^{-2} s^{-1})	**Log_{10} I_{915}** (photons cm^{-2} s^{-1})	**I_{915}** (photons m^{-2} s^{-1})	**Power** (Watts m^{-2})	**Photoisomerization** cone, λ_{abs} = 510 nm (R* $cone^{-1}$ s^{-1})	**Photoisomerization** cone, λ_{abs} = 360 nm (R* $cone^{-1}$ s^{-1})
Mouse retina, cones	5.36E+17	17.73	5.36E+21	1.16E+03	1.32E-02	4.57E-11
	1.81E+18	18.26	1.81E+22	3.93E+03	4.45E-02	1.54E-10
	3.17E+18	18.50	3.17E+22	6.88E+03	7.80E-02	2.70E-10
	4.57E+18	18.66	4.57E+22	9.92E+03	1.12E-01	3.90E-10
	5.97E+18	18.78	5.97E+22	1.30E+04	1.47E-01	5.09E-10
	7.38E+18	18.87	7.38E+22	1.60E+04	1.82E-01	6.29E-10
	8.74E+18	18.94	8.74E+22	1.90E+04	2.15E-01	7.45E-10
Mouse retina, ganglion cells	3.73E+18	18.57	3.73E+22	8.09E+03	9.18E-02	3.18E-10
Mouse V1, cortical neurons	1.68E+15	15.23	1.68E+19	3.65E+00	4.13E-05	1.43E-13
	3.00E+16	16.48	3.00E+20	6.51E+01	7.38E-04	2.56E-12
	4.24E+17	17.63	4.24E+21	9.20E+02	1.04E-02	3.61E-11
	9.33E+17	17.97	9.33E+21	2.02E+03	2.30E-02	7.95E-11
	2.00E+18	18.30	2.00E+22	4.34E+03	4.92E-02	1.71E-10
Mouse behavior	8.48E+17	17.93	8.48E+21	1.84E+03	2.09E-02	7.23E-11
	1.87E+18	18.27	1.87E+22	4.06E+03	4.60E-02	1.59E-10
Human retina	2.25E+15	15.35	2.25E+19	4.88E+00	5.54E-05	1.92E-13
	9.06E+15	15.96	9.06E+19	1.97E+01	2.23E-04	7.72E-13
	1.17E+18	18.07	1.17E+22	2.54E+03	2.88E-02	9.97E-11
	2.46E+18	18.39	2.46E+22	5.34E+03	6.05E-02	2.10E-10
	8.74E+18	18.94	8.74E+22	1.90E+04	2.15E-01	7.45E-10

Table S4. Light intensities. V1 refers to primary visual cortex.